



**HAL**  
open science

# Magnetic signatures of ionospheric disturbance dynamo for CME and HSSWs generated storms

Waqar Younas, C. Amory-mazaudier, Majid Khan, M. Le Huy

► **To cite this version:**

Waqar Younas, C. Amory-mazaudier, Majid Khan, M. Le Huy. Magnetic signatures of ionospheric disturbance dynamo for CME and HSSWs generated storms. *Space Weather: The International Journal of Research and Applications*, 2021, 10.1029/2021SW002825 . hal-03328778

**HAL Id: hal-03328778**

**<https://hal.science/hal-03328778>**

Submitted on 30 Aug 2021

**HAL** is a multi-disciplinary open access archive for the deposit and dissemination of scientific research documents, whether they are published or not. The documents may come from teaching and research institutions in France or abroad, or from public or private research centers.

L'archive ouverte pluridisciplinaire **HAL**, est destinée au dépôt et à la diffusion de documents scientifiques de niveau recherche, publiés ou non, émanant des établissements d'enseignement et de recherche français ou étrangers, des laboratoires publics ou privés.

# 1 Magnetic signatures of ionospheric disturbance dynamo for CME 2 and HSSWs generated storms

3 Waqar Younas<sup>1</sup>, C. Amory-Mazaudier<sup>2,3</sup>, Majid Khan<sup>1</sup>, M. Le Huy<sup>4</sup>

4 <sup>1</sup>Department of Physics, Quaid-i-Azam University Islamabad, Pakistan

5 <sup>2</sup>LPP, CNRS/Ecole Polytechnique/Sorbonne Université/Université Paris-Sud/Observatoire de Paris,  
6 France

7 <sup>3</sup>ICT4D, The Abdus Salam International Centre of Theoretical Physics, Italy

8 <sup>4</sup>Institute of Geophysics, Vietnam Academy of Science and Technology, Hanoi, Vietnam

9

10  
11 Corresponding author: Waqar Younas ([mrwaqar11@gmail.com](mailto:mrwaqar11@gmail.com))

12

13

14

## 15 Key Points

- 16 • A least square fitting method has been used to evaluate the magnetic signatures of ionospheric  
17 disturbance currents and disturbance dynamo electric fields (DDEF).
- 18 • Differences in the magnetic signatures of CME and HSSWs generated magnetic storms are  
19 identified.
- 20 • We have analyzed disturbance dynamo for 19 magnetic storms in three different longitudinal  
21 sectors, as affected by seasonal and longitudinal variations.

22

23

24

This article has been accepted for publication and undergone full peer review but has not been through the copyediting, typesetting, pagination and proofreading process, which may lead to differences between this version and the [Version of Record](#). Please cite this article as doi: [10.1029/2021SW002825](https://doi.org/10.1029/2021SW002825).

This article is protected by copyright. All rights reserved.

## Abstract

25  
26 Ionospheric disturbance dynamo is one of the main processes that causes perturbations in the upper  
27 atmosphere during a magnetic storm. We present a new method, based on the least square fitting,  
28 for estimation of the magnetic signatures associated with ionospheric disturbance currents. Using a  
29 wavelet semblance analysis, the durations of disturbance dynamo electric fields have been  
30 investigated at three longitudinal sectors. For that we have analyzed the disturbance dynamo ( $D_{dyn}$ )  
31 for 19 magnetic storms. It has been found that during CME generated storms magnetic signature of  
32  $D_{dyn}$  may be observed – depending on strength of the storm as well as on the duration of  
33 interplanetary magnetic field (IMF)  $B_z$  southward – in one, two or all three longitudes. The Oscillatory  
34 behavior of IMF  $B_z$  during the high-speed solar wind streams (HSSWs) generates  $D_{dyn}$  globally and the  
35 corresponding effects are observed at all low latitude magnetic observatories. In this regard, the Joule  
36 heating estimation shows that CME and HSSWs generated storms have very different patterns. The  
37  $D_{dyn}$  duration is found to be maximum for the storms occurring during equinox season. Moreover, the  
38 HSSWs events are more likely to cause – because of the oscillatory IMF  $B_z$  – long lasting  $D_{dyn}$  as  
39 compared to CME generated counterpart. This study presents a detailed analysis of disturbance  
40 dynamo as affected by longitudinal and seasonal variations. In this regard the difference in magnetic  
41 signatures, of CME and HSSWs originated storms, have been highlighted.

## Plain Language Summary

42  
43 Space weather activities significantly perturb the quiet time ionosphere through various coupling  
44 mechanisms. Ionospheric disturbance dynamo is one of the main processes that causes perturbations  
45 in the upper atmosphere during a magnetic storm. We present a new method for estimation of the  
46 magnetic signatures associated with ionospheric disturbance currents. The durations of disturbance  
47 dynamo electric fields have been investigated at three longitudinal sectors for 19 magnetic storms. It  
48 has been found that during CME generated storms magnetic signature of  $D_{dyn}$  may be observed in one,  
49 two or all three longitudes. The Oscillatory behavior of IMF  $B_z$  during the high speed solar wind  
50 streams (HSSWs) generates  $D_{dyn}$  globally and the corresponding effects are observed at all low  
51 latitude magnetic observatories. In this regard, the Joule heating estimation shows that CME and  
52 HSSWs generated storms have very different patterns. The  $D_{dyn}$  duration is found to be maximum for  
53 the storms occurring during equinox season. Moreover, the HSSWs events are more likely to cause

54 long lasting  $D_{\text{dyn}}$  as compared to CME generated counterpart. This study presents a detailed analysis  
55 of disturbance dynamo of CME and HSSWs originated storms.

56

57

Accepted Article

## 58 **1. Introduction**

59 It was in 1722, when Graham observed the regular variation of the Earth's magnetic field. It was also  
60 noted that sometimes this variation gets disturbed (Stern, 2002). In 1808 Humboldt introduced the  
61 concept of magnetic storms to understand the magnetic field variations associated with solar  
62 disturbances (Botting, 1994). Balfour Stewart in 1880 presented a possible mechanism to explain the  
63 regular variation of the Earth's magnetic field, where he proposed the circulation of electric currents  
64 above the Earth. The existence of such currents was confirmed by later studies (Stewart, 1880). In  
65 1901, with the first transatlantic link, Marconi demonstrated the existence of ionosphere, in this  
66 regard Breit and Tuve carried a survey of the ionosphere in 1925 (Breit and Tuve, 1925).

67 With increasingly powerful magnetometers the measurements of the magnetic field, on Earth as well  
68 as on board satellites, have become more accurate and the corresponding magnetic data are  
69 interpreted in terms of equivalent electric currents. Incoherent scatter radars allow the  
70 measurements of ionospheric electric currents (Mazaudier, 1982; Mazaudier & Blanc, 1982,  
71 Mazaudier, 1985), e.g. the ones situated at Chatanika in the auroral zone (Brekke et al. 1974), in  
72 middle latitudes at Millstone-Hill/USA and Saint Santin/France (Carpenter and Kirchhoff, 1975;  
73 Mazaudier, 1981; Mazaudier, 1985) and in low latitudes at Arecibo/USA (Harper, 1977). As such  
74 measurements are rare and very expensive, the magnetometer has remained a useful instrument for  
75 describing the real electric currents.

76 Using the theory of the ionospheric regular dynamo (Chapman and Bartels 1940) it is possible to  
77 understand the regular variation of the Earth's magnetic field as generated by the circulation of  
78 neutral atmosphere in the dynamo region (90-150km). The positive ions are preferably driven by the  
79 collisions with neutrals which thus have a speed quite different from electrons, which are under the  
80 sole influence of a Lorentz force. Consequently, there is a creation of electric currents in the  
81 ionosphere (Balfour Stewart's hypothesis; Stewart, 1880).

82 During a magnetic quiet period, the ionospheric regular dynamo is the origin of the Sq (Solar quiet)  
83 and EEJ (Equatorial Electrojet) current systems, respectively at middle and equatorial latitudes.  
84 Whereas for the periods of a robust magnetic activity, strong ionospheric electric currents develop in  
85 the auroral zone. These currents — named as auroral electrojets — dissipate energy by the Joule  
86 heating effect, which in turn modifies the temperature, pressure and movement of the thermosphere.

87 The disturbed thermospheric winds spread towards mid and low latitudes and, by the dynamo effect,  
88 create disturbed ionospheric electric fields, i.e. DDEF. Blanc and Richmond (1980) presented the first  
89 numerical simulation of the Ionospheric disturbance dynamo. In the present study we have focused  
90 on the magnetic signatures of this physical process. Mazaudier and Bernard (1985) observed the  
91 disturbance winds — due to Joule heating — by using the data of incoherent scatter radar, their  
92 findings are consistent with predictions of the Blanc and Richmond model (1980).

93 Another solar wind and/or magnetosphere activity associated with auroral electrojets, and results in  
94 simultaneous penetration of ionospheric electric fields from high to low-latitudes at all longitudes, is  
95 the so-called prompt penetration of the electric field (PPEF) (Nishida 1968). Vasyliunas (1970)  
96 established the first model of the penetration of magnetospheric convection by reproducing the 2  
97 current cells of the DP2 equivalent current system. There are also electric currents in the  
98 magnetosphere (Cole 1966, Fukushima and Kamide 1973) which influence the magnetic observations  
99 around the globe and one needs to remove the effects of these currents while studying ionospheric  
100 dynamics. Thus, the magnetic signature of the disturbed ionospheric dynamo must be extracted from  
101 a complex magnetic signal, which is an integrated effect of different ionospheric and magnetospheric  
102 electric current systems circulating in the terrestrial environment.

103 Fejer et al. (1983) were the first to point out the effect of PPEF and DDEF on incoherent scatter radar  
104 data of Jicamarca. They observed the electric field due to the penetration of the magnetospheric  
105 convection (PPEF) on the day of a magnetic storm, and the electric field due to the disturbed  
106 ionospheric dynamo (DDEF) during the recovery phase of a storm. Likewise, Le Huy and Amory-  
107 Mazaudier (2005) in their study selected the cases having minimum auroral activity during the  
108 recovery phase of storm and thus highlighted the  $D_{dyn}$  magnetic signature of the disturbed ionospheric  
109 dynamo. Zaka et al. (2009) presented the latitudinal variations of disturbance dynamo generated  
110 during the two events of 1993 and compared the results with DP2 disturbance. Fathy et al. (2014)  
111 analyzed the longitudinal variation of disturbance dynamo during the coronal hole event of April 2010.  
112 Fejer et al., (2016) summarized the recent progresses made to analyze the disturbance dynamo and  
113 its effect at middle and low latitudes. Nava et al. (2016), Zaourar et al. (2016), Bulusu et al. (2018) and  
114 Younas et al. (2020) studied the temporal variation of disturbance dynamo generated during different  
115 storms by applying the band pass filter techniques. However, the  $D_{iono}$  can have Sq like variations,  
116 which may not be considered as an effect of DDEF. Hence, applying simple band pass filters to  $D_{iono}$

117 may overestimate the duration of DDEF. Here, we have applied a new method, based on least square  
118 fitting, for the calculations of ionospheric disturbance current. Using a wavelet-based semblance  
119 analysis, we have estimated  $D_{\text{dyn}}$  by separating only those periods which show truly anti-Sq variations.  
120 For that we have analyzed 19 different magnetic storms of various origins.

121 The rest of this article is organized as follows; Section 2 describes the methodology used in this study  
122 while Section 3 presents five events of different categories. In Section 4, we have discussed  $D_{\text{dyn}}$   
123 variations with Joule heating. The summary and conclusion of the study is presented in Section 5.

## 124 **2. Methodology**

### 125 **2.1 Interplanetary Data**

126 Two of the key parameters, namely interplanetary magnetic field (IMF) and solar wind speed,  
127 characterizing the space weather activities are provided by Advanced Composition Explorer  
128 (<http://www.srl.caltech.edu/ACE/>) via OMNIWEB data center (<https://omniweb.gsfc.nasa.gov/>).

### 129 **2.2 Magnetic Indices**

130 The SYM-H, ASYM-H and AE data is obtained from World Data Center for Geomagnetism, Kyoto Japan.  
131 Here SYM-H and ASYM-H indices are, respectively the estimation of symmetric and asymmetric part  
132 of storm-time ring currents, while AE is used to assess auroral currents ([http://wdc.kugi.kyoto-  
133 u.ac.jp/](http://wdc.kugi.kyoto-u.ac.jp/)).

### 134 **2.3 Magnetic observatories and magnetic data analysis**

135 For all the considered 19 magnetic storms, we have analyzed the magnetic data of observatories  
136 located at low latitude in Asian sector (Guam, GUA), African region (M'bour, MBO) and American  
137 sector (Kourou, KOU). For some of the cases we have also included the observations of Adis Ababa  
138 (AAE) and Bac Lieu (BCL). The geographical locations and coordinates of the considered magnetic  
139 observatories are shown, respectively in Fig. 1 and Table 1. The magnetic data of these observatories  
140 is provided by INTERMAGNET (<https://www.intermagnet.org/>).

141 The variation in the horizontal component of magnetic field (H) is used for estimating the ionospheric  
142 disturbance currents ( $D_{\text{iono}}$ ). The H component of magnetic field is computed using the eastward (X)  
143 and northward (Y) components, i.e.,

$$144 \quad H = \sqrt{X^2 + Y^2}$$

145 During a magnetic storm, the  $H$  component of Earth's magnetic field can be decomposed as the  
146 following superposition

$$147 \quad H = H_o + S_q^H + D_{mag} + D_{iono},$$

148 or, equivalently

$$149 \quad D_{iono} = [H - H_o - D_{mag}] - S_q^H \quad (1)$$
$$151 \quad = [\Delta H - D_{mag}] - S_q^H$$

152 Here  $D_{mag}$  is the disturbance due to magnetospheric currents and  $\Delta H = H - H_o$  denoting the  
153 change in  $H$ , after subtracting the corresponding five hours average of local midnight value  $H_o$ . The  
154 disturbance in the  $H$  at low latitudes is mainly influenced by the zonally symmetric ring currents –  
155 whose strength is estimated by the high resolution (1-min) SYMH index. For an accurate investigation  
156 of ionospheric electric field, one needs to remove the effect of these magnetospheric currents from  
157 the magnetic data. For that Choudhary et al. (2001) and Yamazaki et al. (2016) have proposed a least  
158 square technique i.e. by fitting, at a given station, the linear trends to nighttime data of the  $H$   
159 component and SYMH index. The fitting equation can be written as

$$160 \quad H^n = C_1 + C_2 T^n + C_3 SYMH^n, \quad (2)$$

162 where  $T$  is the time in Julian days. Equation (2) is for five hours nighttime data of each day  $n$ . The  
163 coefficients  $C_1$ ,  $C_2$  and  $C_3$  are determined by the method as described below. Consider the equation  
164

$$165 \quad H^n = A^n \times M, \quad (3)$$

167 where  $H^n$  contains the  $H$  data during the nighttime, i.e.  
168

169

$$H^n = \begin{pmatrix} H_1^n \\ H_2^n \\ \vdots \\ H_k^n \end{pmatrix} \quad (4)$$

170

171

172 with  $k$  denoting the total number of nighttime data points and  $A^n$  is a matrix contains the  $T$  and SYMH  
 173 index, as follows

174

$$A^n = \begin{pmatrix} 1 & T_1^n & SYMH_1^n \\ 1 & T_2^n & SYMH_2^n \\ \vdots & \vdots & \vdots \\ 1 & T_k^n & SYMH_k^n \end{pmatrix} \quad (5)$$

175

176 The symbol  $M$  in Eq. (3) depicts a vector which contain the fitting coefficient, namely

177

$$M = \begin{pmatrix} C_1 \\ C_2 \\ C_3 \end{pmatrix} \quad (6)$$

178

179 After calculating  $H^n$  and  $T^n$ , the fitting coefficients can be determined using the least square  
 180 estimation technique (Yamazaki and Maute, 2016). For that one can write

181

$$M = \{(A^n)^t (A^n)^{-1}\} \times \{(A^n)^t (H^n)^{-1}\}, \quad (7)$$

182

183

184 where  $t$  denotes the transpose matrix operation. Once the coefficients  $C_1$ ,  $C_2$  and  $C_3$  are known, the  
 185 corrected variation in  $H$  component can be found by the relation

186

$$[\Delta H - D_{mag}] = H - (C_1 + C_2 \cdot T + C_3 \cdot SYMH) \quad (8)$$

187

188

189 The daily quiet variation (Sq) is calculated from  $\Delta H$  over five quiet days ( $j = 5$ ), i.e.

$$S_q^H = \frac{1}{j} \sum_{i=1}^j \Delta H^i \quad (9)$$

191 Finally, we can determine the desired ionospheric disturbance current ( $D_{iono}$ ) by using Eqs. (8) and (9)  
 192 in Eq. (1).

193 The magnetic disturbance  $D_{iono}$  during a storm can be associated with two phenomena, namely DP2  
 194 and  $D_{dyn}$ . Here the former is a short period magnetic disturbance associated with PPEF (Nishida, 1966)  
 195 and is simultaneously observed at all longitudes during the main phase of a magnetic storm (Nishida,  
 196 1968). Whereas the  $D_{dyn}$  is associated with DDEF (Le Huy and Amory-Mazaudier, 2005; Fathy et al.,  
 197 2014; Bulusu et al., 2018) and results in the anti-Sq oscillations, which are often observed during the  
 198 recovery phase. Moreover, the  $D_{iono}$  has also contribution from other sources such as partial ring  
 199 current during the early phase of a storm and sometime Sq-like oscillations during the recovery phase,  
 200 which cannot be associated  $D_{dyn}$  (Younas et al., 2020). Hence, simply applying filters to  $D_{iono}$  for the  
 201 estimation of  $D_{dyn}$  may not provide an accurate information. Here we propose a wavelet-based  
 202 method, namely semblance analysis (Cooper and Cowan et al., 2008) for the extraction of anti-Sq  
 203 oscillation. Semblance analysis compares the local phase relation between two data sets as function  
 204 of time and wavelength. This can be done by performing a cross wavelet transform (CWT) of two time  
 205 series (Torrence and Compo, 1998) which gives amplitude ( $\alpha$ ) and the local phase ( $\theta = \tan^{-1} \left( \frac{\text{Im}(CWT)}{\text{Re}(CWT)} \right)$ ),  
 206 where Im and Re denotes the imaginary and real parts, respectively. The semblance is then evaluated  
 207 as (Cooper and Cowan et al., 2008)

$$\text{Semblance} = \cos^n(\theta), \quad (10)$$

208  
 209 where  $n$  is a positive odd integer. From above equation it is clear that the semblance ranges from -  
 210 1(anti-correlated) to 1 (positive correlated).

211 Finally,  $D_{dyn}$  can be computed by comparing Sq variation of a station with corresponding  $D_{iono}$  value,  
 212 followed by the extraction of only those periods which are anti-correlated with Sq oscillation, i.e.

$$D_{dyn} = \alpha[\text{anticorr}\{\text{semblance}(Sq, D_{iono})\}] \quad (11)$$

218

219 Here, the function  $semblance(Sq, D_{iono})$  determines the correlation between two signals. Since we  
220 are interested in anti-Sq signatures, thus the contributions having a positive correlation with Sq are  
221 neglected. The factor  $\alpha$  in Eq. (11) denotes a cross-wavelet power amplitude, which quantifies the  
222 strength of anti-correlated periods. The semblance analysis provides a phase correlation between two  
223 signals which ranges from -1 (anti-correlated) to 1 (positive correlated). However, it does not provide  
224 the strength of such correlation (or anti-correlation), e.g. signals A and B can have semblance of -1,  
225 similarly A and C may also have the same semblance, but they can have very different strengths. Such  
226 difference of strength in two signals is quantified by the factor  $\alpha$ , as determined by CWT. Thus, the  
227 semblance is further multiplied by  $\alpha$  to find the relative strength of anti-correlated periods (See Eq. 9  
228 of Cooper and Cowan (2008)). Duration of  $D_{dyn}$  is estimated by considering the time interval from the  
229 start of disturbance till the semblance reduces to a threshold value 0.3, after which there is a weak  
230 anti-correlation and cannot be related to the signatures of  $D_{dyn}$ . In principle, such weak signals remain  
231 non-zero for relatively longer duration.

## 232 2.4 Joule heating of upper atmosphere

233 Joule heating ( $J_H$ ) of upper atmosphere has been estimated through the Space Weather Modeling  
234 Framework (SWMF) version v20140611. We run the SWMF model remotely on Community  
235 Coordinated Modeling Center (CCMC) computers (<http://ccmc.gsfc.nasa.gov>) through various model  
236 runs. The corresponding Joule heating is calculated using height integrated total ionospheric current  
237 ( $J$ ) and Pedersen conductance ( $\sigma_P$ ) as follows (Eyiguler et al., 2018)

238

$$239 \quad J_H = \frac{\sqrt{J_x^2 + J_y^2 + J_z^2}}{\sigma_P} = \frac{J^2}{\sigma_P} \quad (12)$$

240 Here  $J_x, J_y$  and  $J_z$  are ionospheric currents flowing along East, North and upward directions,  
241 respectively.

## 242 3. Results

### 243 3.1 Case – 1

244 Figure 2(a) shows the global parameters, namely (from top to bottom) IMF (nT), Bz component of IMF

245 (nT), solar wind speed (km/s), the AE index (nT), ASYM-H index (nT) and SYM-H index, from 30 March  
246 2001 to 05 April 2001. The arrival of CME, as indicated by sudden storm commencement (SSC), is  
247 shown by a vertical dotted line on 31st March at 0052 UT. The IMF increases rapidly soon after the  
248 SSC and reaches its maximum value of 72 nT at 0122 UT, followed by a gradual decrease during the  
249 late hours of 02 April and eventually returns to its pre-storm value. The CME is associated with an  
250 enhancement in IMF (5.54 to 21.97 nT) as well as in the Bz component of IMF (1.52 to 18.9 nT). Solar  
251 wind speed increases from 420 to 650 km/s, similar trends are observed in SYM-H (-9 nT to 124 nT)  
252 and ASYM-H (10 nT to 128 nT). During this storm, the IMF Bz has started oscillating after the SSC and  
253 at 0530 UT turned southward for a long duration (till 0820 UT) having a minimum value of -49 nT at  
254 0624 UT. The second phase of southward directed Bz started at 1430 UT and remained there till 2210  
255 UT with a minimum value of -36 nT. The main phase (MP) has started at 0440 UT and lasted till 0810  
256 UT with a minimum value of SYM-H index to be -437 nT. During the MP, the AE index has shown a  
257 large increase with a maximum value of 1200 nT. The recovery phase (RP) of this storm started at  
258 0812 UT and lasted till the 04 April with a long period southward directed IMF Bz from 1430UT to  
259 2210 UT on 31<sup>st</sup> March 2001. The AE index shows multiple peaks during the RP with its maximum  
260 value 2407 nT observed at 1711 UT on March 31.

261 Figure 2(b) shows the magnetic variation at (from top to bottom) GUA (Asia), MBO (Africa) and KOU  
262 (America) from 31<sup>st</sup> March to 04 April 2001. Each panel represents  $D_{iono}$  (red), Sq (blue) and SYM-H  
263 index (black). We can observe an anti-Sq signature in  $D_{iono}$  at all the stations on March 31 and 01 April  
264 2001.

265 In Figure 2(c) we present  $D_{dyn}$ , computed using the method as described in Eq. (11), at the three  
266 magnetic observatories, namely GUA, MBO and KOU (top to bottom) from 30 March to 04 April 2001.  
267 Vertical axis presents period of oscillations, where the color bar corresponds to the normalized  
268 strength of  $D_{dyn}$  disturbance at each station. A large enhancement is observed in  $D_{dyn}$ , first in America  
269 followed by Asia and Africa. At the Asian sector,  $D_{dyn}$  has started on April 1 around 0930 UT and lasted  
270 till 1145UT of 03 April with a temporal duration of 2.1 days. Whereas, at the African (American) sector,  
271  $D_{dyn}$  started around 0521 UT 1<sup>st</sup> April (0650 UT on 31<sup>st</sup> of March) and lasted till 1350 UT (1800 UT) 03  
272 April having a temporal duration of around 2.4 (3.5) days. Moreover, we note that the period of  $D_{dyn}$   
273 disturbance is centered around 20 to 28 hours.

### 274 3.2 Case – 2

275 Figure 3(a) present the same analysis as in Fig. 2(a) for a period 15 to 20 March 2013. The CME strikes  
276 the Earth on 17<sup>th</sup> March at 0545 UT as indicated by a vertical dotted line. The compressional phase  
277 (CP) of storm has lasted for 1.5 hours with SYM-H index having a maximum value of 33 nT. The MP  
278 started around 0715 UT and lasted till 2244 UT and SYM-H index reaches a minimum value of -  
279 129nT. The ASYM-H index depicts a large increase with a maximum value of 171 nT at 1230 UT on 17  
280 March 2013. The IMF shows an increasing trend from 4 nT to 22 nT, while Bz component of IMF starts  
281 oscillating in the southward direction and remains there till 2100 UT. The solar wind speed increases  
282 from 420 km/s to 750 Km/s while AE index shows a major auroral activity after the CME with a  
283 maximum peak (2690 nT) observed at 1650 UT.

284 In Fig. 3(b) we present the same analysis as we did for Fig. 2(b) but from 15<sup>th</sup> to 20<sup>th</sup> of March 2015.  
285 This CME strikes at 0545 UT, thus during the MP of the considered storm GUA was on the night side.  
286 The  $D_{iono}$  shows large positive values at GUA. An anti-Sq trend is evident at MBO and KOU on 17 and  
287 18 March 2013, respectively.

288 Figure 3(c) is the same as 1(c) for the period 15 to 18 March 2013. The Asian sector (GUA) does not  
289 show any evidence of  $D_{dyn}$ , whereas we can observe a period of  $D_{dyn}$  disturbance at MBO and KOU,  
290 respectively on 17 and 18 March 2013. Temporal duration of  $D_{dyn}$  at MBO and KOU is 1.5 and 1.2 days,  
291 orderly.

### 292 3.3 Case – 3

293 Figure 4(a) is the same as 1(a) but from 25 to 30 September 2001. The shock of CME, as detected by  
294 SSC, is indicated by a vertical line on 25 September at 1945 UT. The CP of this storm has lasted till  
295 2230 UT (3.5 hours) during which the value of IMF increases from 04 to 36 nT, solar wind speed  
296 changes from 360 to 660 Km/s and ASYM-H index enhances from 20 to 173 nT. The MP has lasted till  
297 0117UT with SYM-H taking its minimum value of -115 nT. The auroral activity remains high till the  
298 mid-day of 26 September 2001 with a maximum peak of 2500 nT at 2215UT on 25 September.

299 Figure 4(b) is same as Fig.(2b) for a period 25 to 30 September 2001. The anti-Sq trend is detected at  
300 GUA station only on 26 September, while MBO and KOU have not shown any anti-Sq oscillation during  
301 the RP. This fact is consistent with Fig. 4(c) which shows that for this particular storm the  $D_{dyn}$   
302 disturbance is found only in the Asian sector (GUA). The duration of  $D_{dyn}$  at GUA is about 1.8 days  
303 (from 25 September 1900 UT to 27 September 1700 UT).

### 304 **3.4 Case – 4**

305 Figure 5 corresponds to the space weather event of 4-10 April 2010. This case has a weak CME at the  
306 beginning with streams of HSSWs lasting till the 10<sup>th</sup> of April 2010. In Fig. 5(a) we present the same  
307 analysis as in Fig. 2(a) but for the period 4 to 10 April 2010. The arrival of a weak CME is marked by  
308 dotted vertical line on 5<sup>th</sup> April 2010 at 0740UT. This CME is associated with an increase in IMF (4 to  
309 21nT), IMF Bz (3 to 18 nT) and the solar wind speed reaches 500 km/s to 810 km/s. Then, IMF Bz  
310 starts oscillating till the 10 April 2010 which is a key indicator of the HSSW streams. The AE index  
311 remained high (1000 nT>) till the 10<sup>th</sup> of April 2010. In Fig. 5(b) the anti-Sq oscillation in  $D_{iono}$  is  
312 observed at all three stations for the whole considered period, which is also confirmed in  $D_{dyn}$  plots,  
313 generated by semblance analysis, in Fig. 5(c). The duration of  $D_{dyn}$  is different at all three longitudes,  
314 e.g. the longest  $D_{dyn}$  disturbance is observed at Africa with the duration of 4.5 days followed by  
315 America and Asia lasting, respectively for 4.2 and 3.9 days.

### 316 **3.5 Case – 5**

317 Figure 6 corresponds to the case of HSSWs that occurred in August 2010. Various global parameters  
318 describing the geomagnetic activity are presented in Fig. 6(a) which is the same as Fig. 2(a) but from  
319 20<sup>th</sup> of August to 31 of August 2010. The arrival of HSSWs is marked by a vertical line dotted line on  
320 23<sup>rd</sup> August at 2313UT. This event is associated with an increase in IMF (6 nT to 22 nT), Bz component  
321 of IMF (0 to 16.7 nT), solar wind speed (285 km/s to 700 km/s) and SYM-H index (18 nT to 59 nT). The  
322 Earth remains under the influence of HSSWs from 23 to 30 August 2010 as indicated by solar wind  
323 speed and oscillatory IMF Bz during a considered period.

324 Figure 6(b) is the same as Fig. 2(b) but for a period 20-29 August 2010. Here one can observe the  
325 presence of anti-Sq signature at all the stations till August 29. Figure 5(c) correspond to  $D_{dyn}$  at three  
326 low latitude stations (GUA, MBO, KOU) located at three longitudinal sectors (Asia, Africa, America)  
327 from 22 to 30 August 2010. The  $D_{dyn}$  disturbance starts first in the Asian sector followed by Africa and  
328 America, respectively. This apparent difference in the response of different sectors might be due to  
329 the local time of the stations. The temporal duration of  $D_{dyn}$  is maximum in Asia, followed successively  
330 by Africa and America.

### 331 **3.6 Comparison among the 5 cases**

332 In the sections 3.1 to 3.5, we have described the geomagnetic activity during the five space weather  
333 events (one from each category). In this regard the cases 1, 2 and 3 correspond to CMEs with  $D_{\text{dyn}}$   
334 observed, respectively at three, two and one sectors, respectively. Whereas for other two cases,  
335 namely 4 and 5 describe the space weather events of CME + HSSWs and HSSWs, respectively. In this  
336 section we look at the possible reasons to explain the observed trends in  $D_{\text{dyn}}$  during these events.

337 During the case of 31<sup>st</sup> March 2001, CME strikes the Earth at 0050UT. The observed  $D_{\text{dyn}}$  is generated  
338 as result of the Joule heating at high latitudes. Figure 7(a) (black) shows the Joule heat – as estimated  
339 by SWMF/BATRUS model – for a period 30<sup>th</sup> March to 02 April 2001, moreover Fig. 7(a) (red)  
340 represents the AE index superimposed on the JH. Here we note the two large sections of Joule  
341 heating with a first peak of 4880 GW as observed on 31 March at 0440UT and a second peak (3320  
342 GW) at 1713 UT. These strong periods of JH generate disturbance dynamo at global scale and  
343 consequently we can observe the anti-Sq signature at all three sectors as indicated in Fig. 2(c).

344 For the event of March 2013, the CME commenced on 17<sup>th</sup> of March at 0406 UT. Figure 7(b) (red)  
345 indicates the variation in JH of upper atmosphere during this space weather event, while the black  
346 curve in the same figure presents AE index variations from 16 March to 19 March 2013. The JH begin  
347 to increase soon after the SSC and remained high till the end of the day (March 17). The maximum  
348 estimated value of JH, using the BATRUS model, is 1180 GW around 1000UT. Heating of upper  
349 atmosphere for long duration generates disturbance dynamo that is observed at low latitudes in two  
350 sectors as indicated in Fig. 2(c).

351 During the magnetic storm of September 2001, CME commenced on 25<sup>th</sup> at 1900 UT. Here we note  
352 that there is a short section of JH having a maximum value of 1600 GW at 2230UT as depicted in  
353 Fig.7(c). This weak JH could not generate disturbance dynamo at global level and is confined to only a  
354 particular sector (as in Fig. 3(c)).

355 For the Case – 4, there is a HSSWs during the recovery phase as indicated by high solar wind speed  
356 and oscillatory IMF  $B_z$ . The arrival of CME is indicated by a vertical line in Fig. 4 on 05 April 0740 UT.  
357 During this event there are two main episodes of JH of upper atmosphere as shown in Fig. 7(d). The  
358 first (second) peak occurred at 0900 (1305) UT having a maximum value of 990 (018) GW. Apart from  
359 these two peaks JH remains relatively high till the mid of 08 April 2010, which is due to the presence  
360 of HSSWs during the recovery phase, which allows energy input for long durations. This JH has  
361 enhanced the duration of  $D_{\text{dyn}}$  at three sectors as observed in Fig. 4(c), i.e. the disturbance lasts for 3.9,  
362 4.5 and 4.2 days, respectively.

363 The last scenario i.e. Case – 5 corresponds to a purely HSSWs event, where the AE index depicts  
364 multiple peaks of energy inputs from 24 to 28 August 2010. Figure 7(e) shows the JH estimation  
365 during the HSSWs this event. Both JH and AE indicate that there is a large energy input from 23  
366 August to 29 August 2010, however magnitude of JH in this case is smaller as compared to the CME  
367 events discussed earlier. The  $D_{dyn}$  started first at Asian sector followed by African and American  
368 counterparts. The temporal duration of observed  $D_{dyn}$  is maximum at Asia and subsequently Africa  
369 and America, respectively. Analysis of these five typical storms shows that during the CME events  
370 disturbance lasts for 1 to 2 days, whereas in case of HSSWs, we see that duration of  $D_{dyn}$  may last for  
371 more than 04 days. The oscillatory IMF Bz for long time, during the HSSWs events, allow long period  
372 of Joule heating in the auroral zone. Furthermore, whenever there is HSSWs along with the CME,  $D_{dyn}$   
373 disturbance is intensified and lasts for several days after the storm.

### 374 **3.7 Generalization to 19 storms**

375 We have computed  $D_{dyn}$  for 19 different space weather events. These considered storms, depending  
376 on the sources (CME/ HSSW/ CME+HSSW/ Several CMEs), are of several categories. Moreover, the  
377 CME events are further categorized with  $D_{dyn}$  observed in 1, 2 or 3 sectors. In Table 2 we have  
378 grouped the cases according to the different categories of events (CMEs, CMEs + HSSW's, HSSWs,  
379 Several CMEs).

380 Table 3, based on the data of Guam, M'Bour and Kourou, presents the results of our analysis for 19  
381 selected events. In the same table columns 1 to 6 show, respectively the type of storm, SSC time in UT,  
382 time of maximum CP with duration, duration of MP with duration, AE peaks with time in UT and  
383 duration of recovery phase. Columns 7 and 8 present the strength and duration of  $D_{dyn}$  at Asian,  
384 African and American sectors, respectively. Figure 8(a) depicts the maximum duration of the observed  
385  $D_{dyn}$  for each storm (from left to right) corresponding to CME only, CME+HSSWs and HSSWs events,  
386 orderly. Here we note that  $D_{dyn}$  duration is largest (from 19 selected events) for the storm 06 (an  
387 HSSWs event). However, it can be inferred from the same figure that duration of  $D_{dyn}$  for HSSWs and  
388 CME+HSSWs events is relatively long as compared to CME (only) events. The mean and standard  
389 deviation are 2.25 days and 0.81 for CME, 4.30 days and 0.72 for CME + HSSW's and 4.30 days and  
390 1.69 for HSSWs. Figure 8(b) presents the maximum strength of  $D_{dyn}$  for each storm (from left to right:  
391 CME only, CME+HSSWs and HSSWs only, respectively). The strength of  $D_{dyn}$  at a station is estimated  
392 by following Le Huy and Amory-Mazaudier (2008), namely from minimum of  $D_{iono}$  when it is anti-  
393 phase to  $S_q$ . Prior to calculating the minimum of  $D_{iono}$ , a moving average filter is applied by following

394 the methodology of Fathy et al., 2014. In this way effect of DP2 magnetic perturbations are averaged  
395 out. The strength of  $D_{dyn}$  is generally high for CME events, e.g. it is large values for storms 5 and 15.  
396 The mean strength and standard deviation are -113.52 nT and 86.16nT for CME, -83.16 nT and 14.68  
397 nT for CME + HSSWs, and -50 nT and 26.27nT for HSSWs. Analysis of Table 3 leads to the following  
398 comments.

- 399 1) for most of the considered cases i.e. 14 out of 19 the  $D_{dyn}$  disturbance is observed in the 3 sectors.
- 400 2) When there is an HSSW (alone or with a CME)  $D_{dyn}$  is observed in the 3 sectors of longitude, in all  
401 the events and the duration of the  $D_{dyn}$  disturbance is longer.
- 402 3) We also note that for the cases of HSSW the peaks of AE are weaker (AE <1000 nT) than for CME  
403 instances (AE from 1200 nT to 2006 nT), however they last for long periods and hence are more  
404 effective in producing  $D_{dyn}$ .

### 405 **3.8 Comparison with Le Huy and Amory-Mazaudier 2005**

406 Le Huy and Amory-Mazaudier have analyzed six magnetic storms (shown in grey in Table 3), by using  
407 3 (different) magnetic observatories (Huancayo in America, Adis Ababa in Africa and Bac Lieu in Asia).  
408 While comparing our findings with the said study, we note that three of the considered storms,  
409 namely 5, 9 and 17 depict the same trends as reported by Le Huy & Amory-Mazaudier 2005. However,  
410 for the events 10, 14 and 16 there are major differences in Asian and American sectors. Thus, we  
411 need to analyze these storms for all the available observatories (Guam, Bac Lieu, Adis Ababa, Mbour,  
412 Kourou and Huancayo) as follows.

413 Figure 9(a) presents the  $D_{dyn}$  at (from top to bottom BCL, GUA, AAE, MBO and KOU during 5 to 8  
414 November 2001 [storm 10 of Table 3] for which Le Huy and Amory-Mazaudier observed the  $D_{dyn}$   
415 signatures at Asian and African sectors. Figure 9(a) shows the signatures of  $D_{dyn}$  at all longitudinal  
416 sectors. Moreover, the stations BCL and GUA – belonging to the same longitudinal sector, namely Asia  
417 – have a different response. This might be due to the fact that  $Sq$  varies, as caused by the planetary  
418 waves, on a daily basis and can affect the evaluation of  $D_{dyn}$  magnetic signatures. At the station AAE  
419 we observe long, as compared to MBO,  $D_{dyn}$  signature. This is probably due to the fact that AAE lies  
420 within EEJ region and has contributions from other physical processes such as enhanced Cowling  
421 conductivity (Cowling, 1932). In the equatorial region – due to the fact that the Earth's magnetic field  
422 is almost horizontal – the conductivity is increased and is called the Cowling's conductivity. Grodji et  
423 al., 2017 described the relations between the various electrodynamic parameters at the equator. In

424 contrast to Le Huy and Amory-Mazaudier (2005) we have observed signature of  $D_{dyn}$  in the American  
425 sector (HUA), this can be due to the use of a different observatory, namely KOU in the same sector.  
426 Figure 9(b) shows the  $D_{dyn}$  (from top to bottom) at GUA, MBO, AAE, KOU and HUA during the storm  
427 14 of Table 3. Here one notes a different signature of  $D_{dyn}$  as compared to Le Huy and Amory-  
428 Mazaudier (2005). There are two possible reasons; first we have employed a different method to  
429 extract  $D_{dyn}$  and second, the use of different observatories in the two studies. Moreover, Le Huy and  
430 Amory-Mazaudier have considered the anti-Sq signature only on the day after the storm.

#### 431 **4. Discussion**

432 Fejer et al. in 1983 studied the signatures of disturbance dynamo electric field over Jicamarca in F-  
433 region during a magnetic quiet day just after a storm, when there was no prompt penetration of the  
434 magnetospheric convection electric field. In the said analysis, they have found perturbed electric  
435 fields around 16-24 hours after the onset of the storm. In a similar study Le Huy and Amory-  
436 Mazaudier considered the ionospheric disturbance dynamo from magnetic data, during a magnetic  
437 quiet day and found the anti-Sq oscillations during the recovery phase.

438 Fathy et al. (2014) studied the disturbance dynamo  $D_{dyn}$  during the coronal hole event of April 2005  
439 and separated the  $D_{dyn}$  perturbation due to the ionospheric disturbance dynamo (Blanc and Richmond,  
440 1980) from DP2 perturbation (Nishida, 1968) which is caused by penetration of the magnetospheric  
441 convection (Vasyliunas, 1970). The separation was achieved by using 4 hours rolling average with a  
442 one-hour step to eliminate the effect of DP2. More recently Zaourar et al. (2017) and Nava et al.  
443 (2016) performed a wavelet analysis on ionospheric disturbance current to estimate the  $D_{dyn}$   
444 perturbation and found that the main disturbance associated with  $D_{dyn}$  has a periodicity of around 20-  
445 28 hours. Younas et al. (2020) recently considered the asymmetric disturbances in the magnetic storm  
446 of August 2018. In this work we have proposed a new approach for the estimation of ionospheric  
447 disturbance current and analyzed 19 storms due to different solar perturbations, i.e. CME, CME +  
448 HSSW and HSSW.

449 Our study reveals several interesting features, which are summarized as following.

450 1. Effect of onset time (UT) and strength of storm for detection of  $D_{dyn}$  during CME generated  
451 storms:

452 Figures 8 (a and b) (left) show duration and strength of  $D_{dyn}$  during the CME generated storms. Here  
453 one notes that, in contrast to HSSWs generated activity, the disturbance dynamo effects are not

454 always observed at all longitudes. Accordingly, we have divided the CME generated storms in three  
455 categories as depicted In Table 2. In Figs. 2, 3 and 4 we have presented storms from each category. Fig.  
456 7 describes the Joule heating estimation and the corresponding AE index. During the CME generated  
457 storm – depending on its strength– IMF B<sub>z</sub> turns southward for long durations and thus allowing large  
458 energy transfer into the magnetosphere. This behavior is quite different from HSSWs generated storm  
459 in which IMF B<sub>z</sub> remains oscillatory. In our case the Joule heating estimates for the three selected  
460 storms have different patterns. For the case 3, there is a sharp pulse of Joule heating, which quickly  
461 drops down to the normal values, while for the cases 1 and 2 Joule heating remains for much longer  
462 intervals. Hence, for the 3<sup>rd</sup> case, the said sharp pulse could not generate the dynamo effect globally  
463 while during the first two cases the large energy input for long time periods generates thermospheric  
464 winds globally. Consequently, the disturbance dynamo becomes strong enough and can be detected  
465 at all three longitudes. Hence, during the CME generated storm duration of IMF B<sub>z</sub> is crucial in  
466 generating D<sub>dyn</sub> globally.

## 467 2. Longitudinal variation of HSSW-generated storms

468 We have analyzed two HSSW events (storms 06 and 19), in this regard Fig. 8(a) shows that, from all  
469 the 19 events, storm 06 has the longest duration of D<sub>dyn</sub>. However, the strength of HSSWs is not  
470 comparable to the CME generated counterparts (Fig. 8b). Both storms have caused D<sub>dyn</sub> effect at all  
471 longitudes, hence interestingly the HSSW-generated storms have long duration of disturbance  
472 dynamo. It looks that oscillatory IMF B<sub>z</sub> frequency plays a key role in the observed signatures of  
473 HSSWs generated storms. As indicated by SYM-H index, the HSSWs events could not generate strong  
474 ring currents. Furthermore, during the HSSWs events IMF B<sub>z</sub> remains oscillatory from the start till the  
475 end of a magnetic storm, which allows energy to be transferred from solar wind to the  
476 magnetosphere in short impulses and lasting for several days. Thus, strong ring current could not  
477 develop during these events. During a CME – in comparison with HSSWs – there is a sudden increase  
478 in auroral activity, which lasts for a short duration and hence may not produce disturbance dynamo  
479 globally. Whereas the continues energy input to auroral ionosphere, during the HSSWs, effectively  
480 heats the polar region and resulting in the signatures of DDEF at all longitudes (Rodriguez Zulaga et al.,  
481 2016).

## 482 483 3. Comparison of results with Le Huy and Amory Mazaudier (2005):

484 We have also presented the comparison of our findings with an earlier study by Le Huy and Amory  
485 Mazaudier (2005) as depicted in Table 3 (gray). For the storms 5, 9 and 17 we have found similar  
486 trends, however for the storms 10, 14 and 16 our findings are quite different. This disagreement is  
487 due to the different methodology and observatories used by Le Huy and Amory -Mazaudier (2005),  
488 who have selected the events for which there was no auroral activity on the day after a magnetic  
489 storm. That means that the associated disturbance DP2, due to the penetration of the electric field,  
490 was zero and only the  $D_{\text{dyn}}$  disturbance – due to the disturbed ionospheric dynamo – was present.  
491 Thus, there was no effect of DP2 and no filtering was required, but this method is only valid for the  
492 day after a storm in certain special cases. However,  $D_{\text{dyn}}$  disturbance can also take place on the day of  
493 storm (some hour after SSC) and is considered in our study.

494

#### 495 4. Effect of season on the duration of storm:

496 The storms 1, 2 and 3 of table 3 occurred in different seasons during the same descending phase of  
497 solar cycle 24. These storms have almost the same origin, i.e. CME with streams of high-speed winds  
498 during the recovery phase. Maximum duration of  $D_{\text{dyn}}$ , as observed from magnetic data, for storms 1,  
499 2 and 3 is 5.2 days, 3.5 and 04 days, respectively. And the maximum strength of  $D_{\text{dyn}}$  for these storms  
500 is, orderly -96 nT, -95.0 nT and -42 nT. This shows that the storms occurring in equinox season are  
501 most likely to have strong and long-lasting disturbance dynamo, which agrees with the theoretical  
502 prediction of Huang (2013). During a magnetic storm large amount of energy deposition, at polar  
503 regions, heats the thermosphere and disturbance thermospheric neutrals winds are generated which  
504 flow towards the equator (Blanc & Richmond, 1980). During the solstice season, there is a  
505 background wind flowing from summer to winter hemisphere which is enhanced during a disturbed  
506 period. Consequently, the equatorward generated storm winds penetrate the winter hemisphere, the  
507 resulting disturbance currents from each hemisphere are not comparable to each other. However, for  
508 the equinox season there is no background wind flowing between the two hemispheres and the  
509 disturbed winds in both hemispheres are comparable, which causes a strong change accumulation at  
510 the equator and thus resulting in strong and long-lasting disturbance dynamo.

511 During the storm 1, AE index reaches a maximum value of 2298 nT on 17<sup>th</sup> March 2015 at 1358 UT  
512 and remained high (>1000 nT) till the end of 22<sup>nd</sup> March. However, for the storm 2, AE index shows a  
513 maximum value of 2698 nT on 22 June at 2009 UT and remained high till the 24<sup>th</sup> of June. For the

514 storm 3, AE index has a maximum value of 2250 nT on 26<sup>th</sup> August 2018 at 0800UT and remained high  
515 till the end of 27<sup>th</sup> August 2018. This indicates that for storm 1, energy inputs to ionosphere-  
516 thermosphere system, as indicated by AE index, remains high for relatively long duration as compared  
517 to storms 2 and 3, which causes a strong and long-lasting disturbance dynamo in the equinox season  
518 (storm 1) in comparison with storms occurring in solstice season (storms 2 and 3).

519

520 5. Main difference in the response to CME, HSSWs and CME+HSSWs generated storms:

521 The  $D_{dyn}$  may be observed in one, two or all sectors depending on the strength, season and starting  
522 UT time of a storm. However, we have found that storm with HSSWs followed by CME or only HSSWs  
523 have shown the effect of  $D_{dyn}$  at all the longitudes, thus making it global. This difference in the  
524 response of CME and HSSWs can be associated with oscillatory IMF  $B_z$  which allows continuous energy  
525 input to the magnetosphere-ionosphere system and thus heating of the upper atmosphere. Whereas,  
526 during the CME events, IMF  $B_z$  turns southward and thus allowing large energy transfer. However, in  
527 contrast to HSSWs, such events last for short durations and hence do not generate enough Joule  
528 heating to cause a global  $D_{dyn}$ . This effect is evident during the weak CME events as illustrated in Table  
529 3.

## 530 5. Conclusion

531 To conclude, we have analyzed the magnetic signatures of ionospheric disturbance dynamo ( $D_{dyn}$ )  
532 with a new method. In this regard the analysis has been performed for 19 different space weather  
533 events, for which we have found some interesting features of  $D_{dyn}$  which are summarized as follows.

- 534 1. The period of  $D_{dyn}$  oscillations is found to be between 16 and 28 hours, which agrees with  
535 some earlier theoretical predictions (Rodríguez-Zuluaga et al.,2016; Huang, 2012).
- 536 2. The  $D_{dyn}$  during the CME generated storms may be observed, depending on the strength of  
537 storm, in one, two or three longitudinal sectors. This fact can be related to southward  
538 excursion of IMF  $B_z$ . The storm with very long period of IMF  $B_z$ , or more than one episode of  
539 southward directed IMF  $B_z$ , may result in a global generation of  $D_{dyn}$ , which generates the  
540 observed magnetic signatures at all longitudes.
- 541 3. In contrast to CME generated event, the  $D_{dyn}$  during HSSWs or CME+HSSWs is detected at  
542 all longitudes. This effect is related with the oscillatory behavior of IMF  $B_z$  during the HSSWs,

543 which allows continuous energy to build up in the thermosphere. Furthermore, the HSSWs  
544 generated storms are most likely to have long duration of  $D_{\text{dyn}}$ .

545 4. Our analysis of three magnetic storms, having almost the same global variations, reveals  
546 that the storms occurring in the equinox season are expected to have a strong  $D_{\text{dyn}}$  as  
547 compared to events in other seasons.

548 5. The magnetic storms with multiple CMEs show multiple episodes of  $D_{\text{dyn}}$  and can be  
549 associated with corresponding episodes of IMF  $B_z$  southward.

550 6. Joule heating analysis from AE index and BATRUS model indicates that the CME, HSSWs and  
551 CME+HSSW events have quite different heating patterns of the upper atmosphere. The CME  
552 events that have  $D_{\text{dyn}}$  in only one longitude show sharp and short duration of high energy  
553 input. Conversely, the HSSW and CME+HSSW-generated storms have long duration of Joule  
554 heating. Probably, this is the reason why HSSW-generated storms tend to have long duration  
555 of  $D_{\text{dyn}}$ .

556 This study emphasizes that HSSW-driven events usually could not develop strong ring currents  
557 which is a proxy to measure the strength of a magnetic storm. However, these events may cause  
558 significant perturbation in the ionosphere-thermosphere through penetration of electric fields  
559 from high to low latitudes for several days. Hence, HSSWs should be taken into account while  
560 modeling and estimating ionosphere response during disturbed periods.

## 561 **Acknowledgement**

562 We would like to thank INTERMAGNET(<https://www.intermagnet.org/>) for providing magnetic data,  
563 OMNIWEB (<https://omniweb.gsfc.nasa.gov/>) for providing interplanetary data and World Data Center  
564 (WDC)(<http://wdc.kugi.kyoto-u.ac.jp/>) Kyoto for providing magnetic indices. SWMF/BATSRUS tools  
565 developed at the University of Michigan Center for Space Environment Modeling (CSEM) and made  
566 available through the NASA Community Coordinated Modeling Center (CCMC) through their public  
567 Runs on Request system (<http://ccmc.gsfc.nasa.gov>). The CCMC is a multiagency partnership between  
568 NASA, AFMC, AFOSR, AFRL, AFWA, NOAA, NSF, and ONR. Authors thank the ISSI-Bern International  
569 Team of ‘Why Ionospheric Dynamics and Structure Behave Differently in The African Sector?’ (The  
570 team leaders E. Yizengaw& K. Groves) for a valuable discussion about part of the result that is  
571 included in this paper. W. Younas thanks to L. Rastätter from Community-Coordinated Modeling

572 Center, NASA Goddard Space Flight Center, Greenbelt, MD, USA for coordinating in conducting SWMF  
573 model runs remotely and proofreading of manuscript.

574

575

576

Accepted Article

577 **References**

578

- 579 Amory-Mazaudier, C., Bolaji, O. S., & Doumbia, V. (2017). On the historical origins of the CEJ, DP2, and Ddyn current  
580 systems and their roles in the predictions of ionospheric responses to geomagnetic storms at equatorial  
581 latitudes. *Journal of Geophysical Research: Space Physics*, 122(7), 7827–7833.  
582 <https://doi.org/10.1002/2017ja024132>
- 583 Blanc, M., & Richmond, A. D. (1980). The ionospheric disturbance dynamo. *Journal of Geophysical Research*, 85(A4),  
584 1669. <https://doi.org/10.1029/ja085ia04p01669>
- 585 Botting, D. (1994), *Humboldt and the Cosmos*, 323 pp., Prestel, Munich, Germany
- 586
- 587 Brekke, A., Doupnik, J. R., & Banks, P. M. (1974). Incoherent scatter measurements of Eregion conductivities and  
588 currents in the auroral zone. *Journal of Geophysical Research*, 79(25), 3773–3790.  
589 <https://doi.org/10.1029/ja079i025p03773>
- 590 BREIT, G., & TUVE, M. A. (1925). A Radio Method of Estimating the Height of the Conducting Layer. *Nature*,  
591 116(2914), 357–357. <https://doi.org/10.1038/116357a0>
- 592 Bulusu, J., R. K., A., Arora, K., Chandrasekhar, N. P., & Nagarajan, N. (2018). Effect of disturbance electric fields on  
593 equatorial electrojet over Indian longitudes. *Journal of Geophysical Research: Space Physics*, 123.  
594 <https://doi.org/10.1029/2018JA025247>
- 595 Chapman, S., & J. Bartels (1940), *Geomagnetism*, Oxford University Press, New York.
- 596 Choudhary, R. K., St.-Maurice, J.-P., Ambili, K. M., Sunda, S., & Pathan, B. M. (2011). The impact of the January 15,  
597 2010, annular solar eclipse on the equatorial and low latitude ionospheric densities. *Journal of Geophysical*  
598 *Research: Space Physics*, 116(A9), n/a-n/a. <https://doi.org/10.1029/2011ja016504>
- 599 Carpenter, L. A., & Kirchhoff, V. W. J. H. (1975). Comparison of high-latitude and mid-latitude ionospheric electric  
600 fields. *Journal of Geophysical Research*, 80(13), 1810–1814. <https://doi.org/10.1029/ja080i013p01810>
- 601 Cole, K. D. (1966). Magnetic storms and associated phenomena. *Space Science Reviews*, 5(6), 699–770.  
602 <https://doi.org/10.1007/bf00173103>
- 603 Cooper, G. R. J., & Cowan, D. R. (2008). Comparing time series using wavelet-based semblance analysis. *Computers*  
604 *& Geosciences*, 34(2), 95–102. <https://doi.org/10.1016/j.cageo.2007.03.009>
- 605 Cummings, W. D. (1966). Asymmetric ring currents and the low-latitude disturbance daily variation. *Journal of*  
606 *Geophysical Research*, 71(19), 4495–4503. <https://doi.org/10.1029/jz071i019p04495>

- 607 Cowling, T. G. (1932). The Electrical Conductivity of an Ionised Gas in the Presence of a Magnetic Field. Monthly  
608 Notices of the Royal Astronomical Society, 93(1), 90–97. <https://doi.org/10.1093/mnras/93.1.90>  
609
- 610 Fathy, I., Amory-Mazaudier, C., Fathy, A., Mahrous, A. M., Yumoto, &Ghamry, E. (2014). Ionospheric disturbance  
611 dynamo associated to a coronal hole: Case study of 5–10 April 2010, J. Geophys. Res. SpacePhysics, 119, 4120–  
612 4133, <https://doi.org/10.1002/2013JA019510>
- 613 Fejer, B. G., Larsen, M. F., &Farley, D. T. (1983). Equatorial disturbance dynamo electric fields. Geophysical Research  
614 Letters, 10(7), 537–540. <https://doi.org/10.1029/gl010i007p00537>
- 615 Fukushima, N., &Kamide, Y. (1973). Partial ring current models for worldwide geomagnetic disturbances. Reviews of  
616 Geophysics, 11(4), 795. <https://doi.org/10.1029/rg011i004p00795>
- 617 Fuller-Rowell, T. J., Codrescu, M. V., Moffett, R. J., &Quegan, S. (1994). Response of the thermosphere and  
618 ionosphere to geomagnetic storms. Journal of Geophysical Research, 99(A3), 3893.  
619 <https://doi.org/10.1029/93ja02015>
- 620 Fuller-Rowell, T. J., Codrescu, M. V., Rishbeth, H., Moffett, R. J., &Quegan, S. (1996). On the seasonal response of the  
621 thermosphere and ionosphere to geomagnetic storms. Journal of Geophysical Research: Space Physics, 101(A2),  
622 2343–2353. <https://doi.org/10.1029/95ja01614>
- 623 Fuller-Rowell, T. J., Millward, G. H., Richmond, A. D., & Codrescu, M. V. (2002). Storm-time changes in the upper  
624 atmosphere at low latitudes. Journal of Atmospheric and Solar-Terrestrial Physics, 64(12–14), 1383–1391.  
625 [https://doi.org/10.1016/s1364-6826\(02\)001013](https://doi.org/10.1016/s1364-6826(02)001013).
- 626 Grodgi, F., V. Doumbia, K. Boka, C. Amory-Mazaudier, Y. Cohen, R. Fleury, 2017, Estimating some parameters of the  
627 equatorial ionosphere electrodynamic from ionosonde data in West Africa in Advances and Space Research  
628 <http://dx.doi.org/10.1016/j.asr.2016.09.004>, ASR, 59, p 311-325
- 629 Harper, R. M. (1977). Tidal winds in the 100- to 200-km region at Arecibo. Journal of Geophysical Research, 82(22),  
630 3243–3250. <https://doi.org/10.1029/ja082i022p03243>
- 631 Huang, C. M. (2013). Disturbance dynamo electric fields in response to geomagnetic storms occurring at different  
632 universal times. Journal of Geophysical Research: Space Physics, 118(1), 496–501.  
633 <https://doi.org/10.1029/2012ja018118>
- 634 Kashcheyev, A., Migoya-Oru , Y., Amory-Mazaudier, C., Fleury, R., Nava, B., Alazo-Cuartas, K., &Radicella, S. M.  
635 (2018). Multivariable Comprehensive Analysis of Two Great Geomagnetic Storms of 2015. Journal of  
636 Geophysical Research: Space Physics, 123(6), 5000–5018. <https://doi.org/10.1029/2017ja024900>

- 637 KalafatogluEyiguler, E. C., Kaymaz, Z. Frissell, N. A., Ruohoniemi, J. M., &Rastätter, L. (2018). Investigating upper  
638 atmospheric Joule heating using cross-combination of data for two moderate substorm cases. *Space*  
639 *Weather*, 16, 987–1012. <https://doi.org/10.1029/2018SW001956>
- 640 Le Huy, M. and Amory-Mazaudier, C. (2005). Magnetic signature of the ionospheric disturbance dynamo at  
641 equatorial latitudes: “Ddyn.” *Journal of Geophysical Research*, 110(A10).  
642 <https://doi.org/10.1029/2004ja010578>
- 643 Mazaudier, C. (1982). Electric currents above Saint-Santin: 1. Data. *Journal of Geophysical Research*, 87(A4), 2459.  
644 <https://doi.org/10.1029/ja087ia04p02459>
- 645 Mazaudier, C., & Blanc, M. (1982). Electric currents above Saint-Santin: 2. Model. *Journal of Geophysical Research*,  
646 87(A4), 2465. <https://doi.org/10.1029/ja087ia04p02465>
- 647 Mazaudier, C. (1985). Electric currents above Saint-Santin: 3. A preliminary study of disturbances: June 6, 1978;  
648 March 22, 1979; March 23, 1979. *Journal of Geophysical Research*, 90(A2),  
649 1355. <https://doi.org/10.1029/ja090ia02p01355>
- 650 Mazaudier C. R. Bernard, Saint-Santin radar observations of lower thermospheric storms, *J. Geophys. Res.*, 90 (A3),  
651 2885-2895, 1985
- 652 Nava, B., Rodríguez-Zuluaga, J., Alazo-Cuartas, K., Kashcheyev, A., Migoya-Orué, Y., Radicella, S. M., Amory-  
653 Mazaudier, C., & Fleury, R. (2016). Middle- and low-latitude ionosphere response to 2015 St. Patrick’s Day  
654 geomagnetic storm. *Journal of Geophysical Research: Space Physics*, 121(4), 3421–3438.  
655 <https://doi.org/10.1002/2015ja022299>
- 656 Nishida, A. (1968). Geomagnetic DP 2 fluctuations and associated magnetospheric phenomena. *J. Geophys. Res.*, 73,  
657 1795–1803, doi: 10.1029/JA073i005p01795.
- 658 Nishida, A., N. Iwasaki, and N. T. Nagata (1966). The origin of fluctuations in the equatorial electrojet: A new type of  
659 geomagnetic variation. *Ann. Geophys.*, 22, 478–484.
- 660 Rishbeth, H. (1989), Basic physics of the ionosphere, in *Radio-Wave Propagation*, edited by M. P. M. Hall and L. W.  
661 Barclay, pp. 75–94, Peter Peregrinus, London
- 662 Richmond, A. D., and R. G. Roble (1979), Dynamic effects of aurora generated gravity waves on the mid-latitude  
663 ionosphere, *J. Atmos. Terr. Phys.*, 41, 841–852
- 664 Rodríguez-Zuluaga, J., Radicella, S. M., Nava, B., Amory-Mazaudier, C., Mora-Páez, H., &Alazo-Cuartas, K. (2016).  
665 Distinct responses of the low-latitude ionosphere to CME and HSSWS: The role of the IMF Bz oscillation

666 frequency. *Journal of Geophysical Research: Space Physics*, 121(11), 11,528-11,548.  
667 <https://doi.org/10.1002/2016ja022539>

668 Stern, D. P. (2002), A millennium of geomagnetism, *Rev. Geophys.*, 40(3), 1007, doi:10.1029/2000RG000097

669 Stewart, B. (1880). On Some Points Connected with Terrestrial Magnetism. *Nature*, 22(557), 202–203.  
670 <https://doi.org/10.1038/022202a0>

671 Testud, J., and G. Vasseur (1969), Ondes de gravité dans la thermosphère, *Ann. Geophys.*, 25, 525–546

672 Torrence, C., & Compo, G. P. (1998). A Practical Guide to Wavelet Analysis. *Bulletin of the American Meteorological*  
673 *Society*, 79(1), 61–78. [https://doi.org/10.1175/1520-0477\(1998\)079<0061:apgtwa>2.0.co;2](https://doi.org/10.1175/1520-0477(1998)079<0061:apgtwa>2.0.co;2)

674 Vasyliunas, V. M. (1970), Mathematical models of magnetospheric convection and its coupling to the ionosphere, in  
675 *Particles and Fields in the Magnetosphere*, edited by M. McCormac, pp. 60– 71, Springer, New York.

676 Vasyliunas, V. M. (1972), The interrelationship of magnetospheric processes, in *Earth's Magnetosphere Processes*,  
677 edited by B. M. McCormac, pp. 29-38, D. Reidel, Norwell, Mass.

678 Yamazaki, Y., & Maute, A. (2016). Sq and EEJ—A Review on the Daily Variation of the Geomagnetic Field Caused by  
679 Ionospheric Dynamo Currents. *Space Science Reviews*, 206(1–4), 299–405. [https://doi.org/10.1007/s11214-](https://doi.org/10.1007/s11214-016-0282-z)  
680 [016-0282-z](https://doi.org/10.1007/s11214-016-0282-z)

681 Younas, W., Amory-Mazaudier, C., Khan, M., & Fleury, R. (2020). Ionospheric and Magnetic Signatures of a Space  
682 Weather Event on 25–29 August 2018: CME and HSSWs. *Journal of Geophysical Research: Space Physics*, 125(8).  
683 <https://doi.org/10.1029/2020ja027981>

684 Zaourar, N., Amory-Mazaudier, C., & Fleury, R. (2017). Hemispheric asymmetries in the ionosphere response  
685 observed during the high-speed solar wind streams of the 24–28 August 2010. *Advances in Space Research*,  
686 59(9), 2229–2247. <https://doi.org/10.1016/j.asr.2017.01.048>

687 Zaka, K. Z., Koba, A. T., Doumbia, V., Richmond, A. D., Maute, A., Mene, N. M., et al. (2010). Simulation of electric  
688 field and current during the 11 June 1993 disturbance dynamo event: Comparison with the observations.  
689 *Journal of Geophysical Research: Space Physics*, 115(A11), n/a-n/a. <https://doi.org/10.1029/2010ja015417>

690

691

692

## Table captions

693

694 **Table 1:** Geomagnetic and geographic coordinates of the considered magnetic observatories.

695

696 **Table 2:** Classification of selected storms into different categories based on source, CME events with DD  
697 observed at 3, 2 and 1 sectors, CME+HSSWs, HSSWs only and cases with several CMEs.

698 **Table 3:** Statistical analysis of  $D_{\text{dyn}}$  observed at three sectors during 19 different magnetic storms.

699

700

701

## Figure captions

702

703

704 **Figure 1:** Location of the magnetic observatories.

705 **Figure 2: a)** Global Parameters, (from top to bottom): IMF in nano tesla, Bz component of IMF in nano tesla,  
706 solar wind speed in Km/s, AE index in nano tesla, ASYM-H index in nano tesla and SYM-H in nano tesla from 30  
707 March to 05 April 2001. **b)** Magnetic variations at three observatories located in three regions (from top to  
708 bottom): GUA [Asia], MBO [Africa] and KOU [America] from 30 March to 04 April 2001. On each panel Delta H  
709 (black), Sq variation (blue) and disturbed ionospheric current  $D_{iono}$  is superimposed. **c)** Disturbance dynamo  
710 ( $D_{dyn}$ ) estimated using wavelet based semblance analysis during 30 March to 04 April 2001. The vertical dashed  
711 line corresponds to the arrival of CME.

712 **Figure 3: a)** Same as Fig. 1(a) but from 15 to 19 March 2013, **b)** same as Fig 1(b) but 15 to 19

713 March 2013, **c)** same as Fig 1(c) but 15 to 18 March 2013.

714 **Figure 4: a)** Same as Fig. 1(a) but from 25 to 30 September 2001, **b)** same as Fig 1(b) but from 25-29 September  
715 2001, **c)** same as Fig 1(c) but 25 to 29 September 2001

716 **Figure 5: a)** Same as Fig. 1(a) but 4 to 10 April 2010, **b)** same as Fig 1(b) but 04 to 10

717 April 2010, **c)** same as Fig 1(c) but 04 to 10 April 2010.

718 **Figure 6: a)** Same as Fig. 1(a) but 20 to 31 August 2010, **b)** same as Fig 1(b) but 20 to 29 August 2010, **c)** same  
719 as Fig 1(c) but 22 to 30 August 2010.

720 **Figure 7:** Comparison between AE and Joule heating for the 5 selected events.

721 **Figure 8: a)** Maximum duration of  $D_{dyn}$  during each of the selected storm: (from left to right) CME, CME+HSSWs  
722 and HSSWs events respectively. **b)** Maximum strength of  $D_{dyn}$  observed during each storm.

723 **Figure 9 :** The  $D_{dyn}$  disturbance **a)** storm of November 6, 2001 and **b)** storm of September 25, 2001

724

725

Accepted Article

726

727

728

729

730

**Table 1**

<b>Station ID</b>	<b>Sector</b>	<b>Latitude</b>	<b>Longitude</b>	<b>Magnetic dip</b>
GUA	Asia	13.59	144.87	12.35
BCL	Asia	9.28	105.73	1.33
AAE	Africa	9.03	38.76	0.43
MBO	Africa	14.38	-16.97	6.99
KOU	America	5.21	-52.93	15.25
HUA	America	-12.05	-75.01	0.62

731

732

733

734

735

736

737

738

739

740

741

742

743

744

745  
746  
747  
748  
749

**Table 2**

1 CME			Several CME	CME + HSSW	HSSW
1 Longitude sector	2 Longitude sectors	3 Longitude sectors			
25-Sep 2001 (09)	Nov 2003 (15)	March -April 2001 (05)	Nov.2004 (12)	April 2010 (04)	August 2010 (06)
Oct 2000(16)	March 2013 (18)	May 2017 (07)	July 2004 (13)	March2015(01)	April 2005 (19)
		April 2012 (08)		June2015 (02)	
		Dec 2006 (11)		August2018 (03)	
		24 Nov 2001 (17)			
		6 Nov 2001 (10)			
		23 Sep 2001 (14)			

750  
751  
752  
753  
754  
755  
756  
757  
758  
759  
760  
761  
762  
763

764

765

Accepted Article

**Table 3**

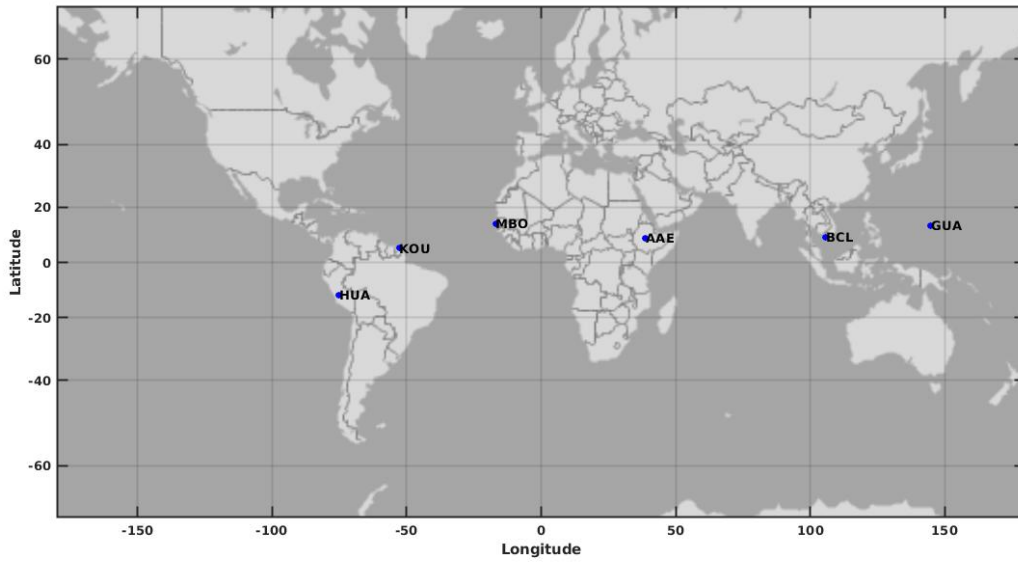
No	SSC [UT] YYYY-MM-DD HH-MIN LT times in Asia, Africa America	UT Time and Max. of CP  (Positive SYMH[nT])  + duration	UT Time and Max. of MP  (negative SYMH)  + duration	UT time and max. AE (nT)  YYYYMMDD-HHMM AE(nT)	Duration of the RP [Days]	D <sub>dyn</sub> duration with Start and end time in UT			Maximum Strength of D <sub>dyn</sub> with UT time in each Sector		
						Asia	Africa	America	Asia	Africa	America
Storm 1 CME + HSSW	2015-03-17- 0445 UT  Asia [12 :00 LT]  Africa [03 :30 LT]  America [01 :15 LT]	0448 UT (67)  02 Hours	2245 UT (-230 nT)  16 Hours	20150317-0830 (778 )  20150317-1430 (1570 )  20150317-1830 (1260 )  20150317- 2330(1170)	7.5 Days	17/03 1600 UT  19/03 0500 UT  1.5 Days	18/03 0300 UT  23/03 0800 UT  5.2Days	18/03 0200 UT  22/03 1300 UT  4.5Days	18/03/15  0220UT  -45.7nT	17/03/15  1731UT  <b>-96nT</b>	17/03/15  2141UT  -79nT
Storm 2 CME + HSSW	2015-06-22- 1822 UT  Asia [01 :00 LT]  Africa [17 :00 LT]  America [15 :45 LT]	0622 1838 UT (85 )  01 Hours	06230425 UT (-207 nT)  10 Hours	20150622-1830 (1636 )  20150623-1230 (1346 )	7.5 Days	23/06 0600 UT  27/06 0100 UT  3.8Days	23/06 0200 UT  27/06 0200 UT  4 Days	23/06 0500 UT  26/06 1400 UT  3.5 Days	23/06/15  1115UT  -25nT	23/06/15  1350UT  <b>-95.0nT</b>	22/06/15  2140UT  -51.79nT
Storm 3 CME + HSSW	2018-08-25 0750 UT  Asia [14 :00 LT]  Africa [06 :00 LT]	0825 0832 UT 27  09 Hours	08260711 UT (-206 nT)  17 Hours	NA	7.5 Days	26/08 2200  27/08 1500  0.8 Days	26/08 1600  30/08 0200  3.5 Days	26/08 1200  28/08 2300  2.5 Days	26/08/18  1755UT  -17.4nT	26/08/18  1639UT  <b>-42.8nT</b>	26/08/18  1759UT  -37.61nT

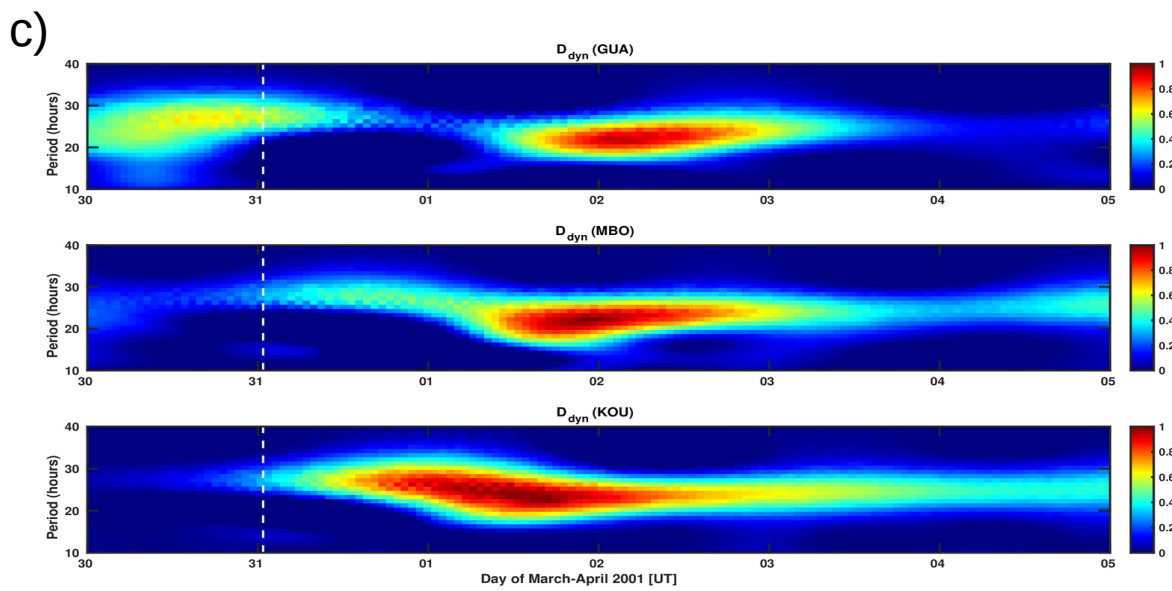
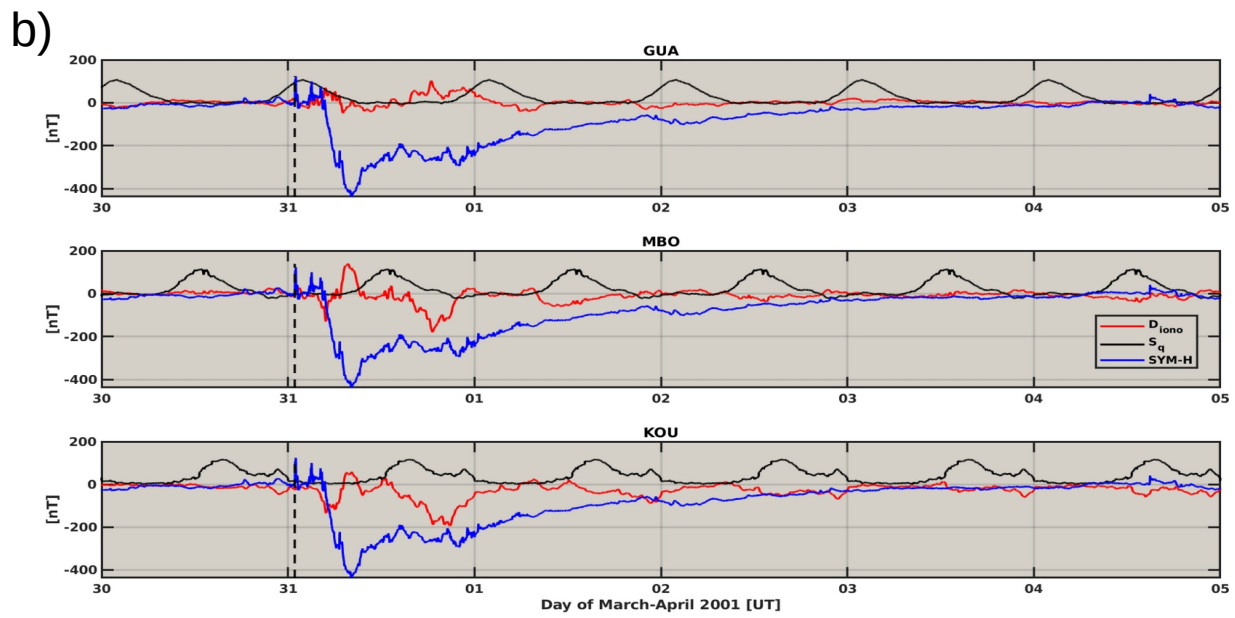
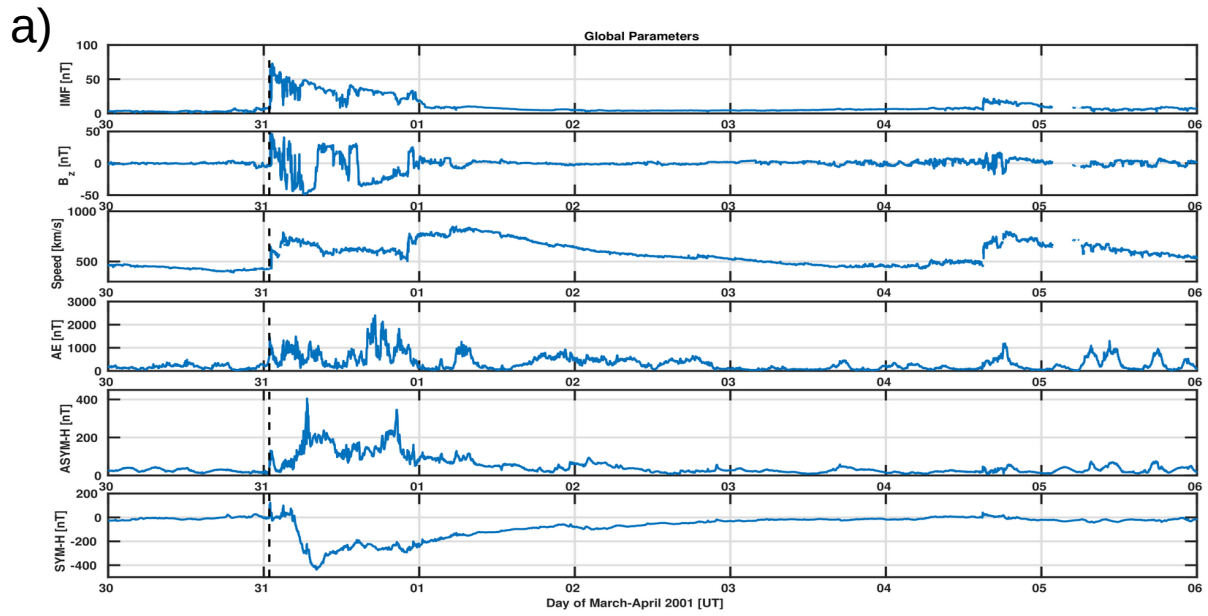
	America [04 :30 LT]											
Storm 4 CME + HSSW	2010-04-05- 0730 UT Asia [14 :00 LT] Africa [06 :00 LT] America [04 :30 LT]	0504 0830 UT 28 02 Hours	0604 0740 UT -90 nT 22 Hours	20100405-0930 (1419 ) 20100406-1430 (1290 )	4.7 Days	05/04 2200 09/04 2000 3.9 Days	05/04 1300 10/04 0700 4.5 Days	05/04 0900 10/04 1300 4.2 Days	07/04/10 0240UT -30 nT	06/04/10 1245UT <b>-64nT</b>	06/04/10 1555UT -39.8nT	
Storm 5 CME	2001-03-31- 0050 UT Asia [08 :20 LT] Africa [23 :30 LT] America [21:30 LT]	3103 0100 124 03 Hours	3103 0812 -435 nT 07 Hours	20010331-0330 (936 ) 20010331-1630 (1524 ) 20010331-1830 (1503 )	05 Days	01/04 0937 03/04 1146 2.1 Days	01/04 0521 03/04 1354 2.4 Days	31/03 0650 03/04 1354 3.5 Days	01/04/01 0625UT -31.7nT	31/03/01 1905UT <b>-115.4nT</b>	31/03/01 1930UT -167nT	
Storm 6 HSSW	2010-08-23- 1300 UT Asia [21:00 LT] Africa [11 :30 LT] America [09 :30 LT]	2308 2244 59 11 Hours	2508 0440 -40 nT 29 Hours	20100824-0030 (450) 20100824-1230 (660) 20100825-0330 (824) 201008251130 (560) 20100825 2330 (500 ) 20100827 0630 (500)	05 Days	24/08 0300 29/08 1730 5.5 Days	24/08 2045 28/08 0000 3.3 Days	25/08 0630 28/08 0200 2.8 Days	24/08/10 0400UT <b>-25nT</b>	25/08/10 1410UT -20.66nT	25/08/10 0120UT -10.2nT	
Storm 7 CME	2017-05-27- 1533 Asia [23:00 LT] Africa [14 :00 LT]	2705 2118 58 7.5 Hours	2805 0714 -142 nT 10 Hours	20170528-0530 (1271)	04 Days	29/05 0800 30/05 1300 1.3 Days	28/05 0400 31/05 1400 3.5 Days	29/05 0100 01/06 0100 03 Days	28/05/17 0845UT -48nT	28/05/17 1500UT -52nT	29/05/17 1530UT <b>-58nT</b>	

	America [12 :00 LT]										
Storm 8 CME	2012-04-23-0310 UT Asia [11:00 LT] Africa [01 :40 LT] America [23 :50 LT]	2304 0423 44 15 Hours	2405 0330 -124 nT 09 Hours	20120412-1930 (990)	3.8 Days	25/04 1600 29/04 1000 3.5 Days	24/04 1300 27/04 1600 3.1 Days	24/04 0900 27/04 1900 3.5 Days	24/04/12 0245UT -20.2nT	25/04/12 1050UT <b>-40.0nT</b>	24/04/12 1710UT -28.8nT
Storm 9 CME	2001-09-25-1945 UT Asia [03:00 LT] Africa [18 :30 LT] America [15 :15 LT]	2509 2200 46 2.5 Hours	2609 0110 -118 nT 2.5 Hours	20010925-2230 (1753)	4.8 Days	25/09 1900 27/09 1700 1.8 Days	NA NA	NA NA	25/09/01 2310UT -48.98nT	NA\ NA	NA
Storm 10 CME	2001-11-06-0153 UT Asia [20:00 LT] Africa [00 :30 LT] America [22 :30 LT]	0611 0154 27 20 Min	0611 0406 -320 nT 02 Hours	20011106-0430 (1990)	4.9 Days	NA 08/11 0300 1.5 Days	06/11 1600 07/11 2000 1.1 Day	06/11 1800 07/11 2000	06/11/01 0500UT <b>-35nT</b>	07/11/01 0750UT -24.2nT	06/11/01 1810UT -21nT
Storm 11 CME	2006-12-14-1400 UT Asia [07:00 LT] Africa [12 :30 LT] America [10 :30 LT]	1412 2110 UT 19 02 Hours	1512 0055 -211 nT 02 Hours	20061214-1530 (1616) 20061215-0230 (1290) 20061215-0930 (1372)	06 Days	14/12 2300 UT 19/12 1500 UT 4.5 Days	14/12 1800 16/12 1900 2.1 Days	14/12 1900 17/12 2000 03 Days	16/12/06 0245UT -15nT	15/12/06 1350UT <b>-102nT</b>	15/12/06 1600UT -55.7nT
Storm 12 Multiple	2004-11-07-1740 UT	0711 1940 UT	0811 0555 UT -395 nT	20041108-0130 (1303) 20041108-0430	06 Days	09/11 0600 12/11 0300	08/11 0100 12/11 0200	08/11 0500 11/11 1900	10/11/04 0730UT	09/11/04 1410UT	09/11/04 2120UT

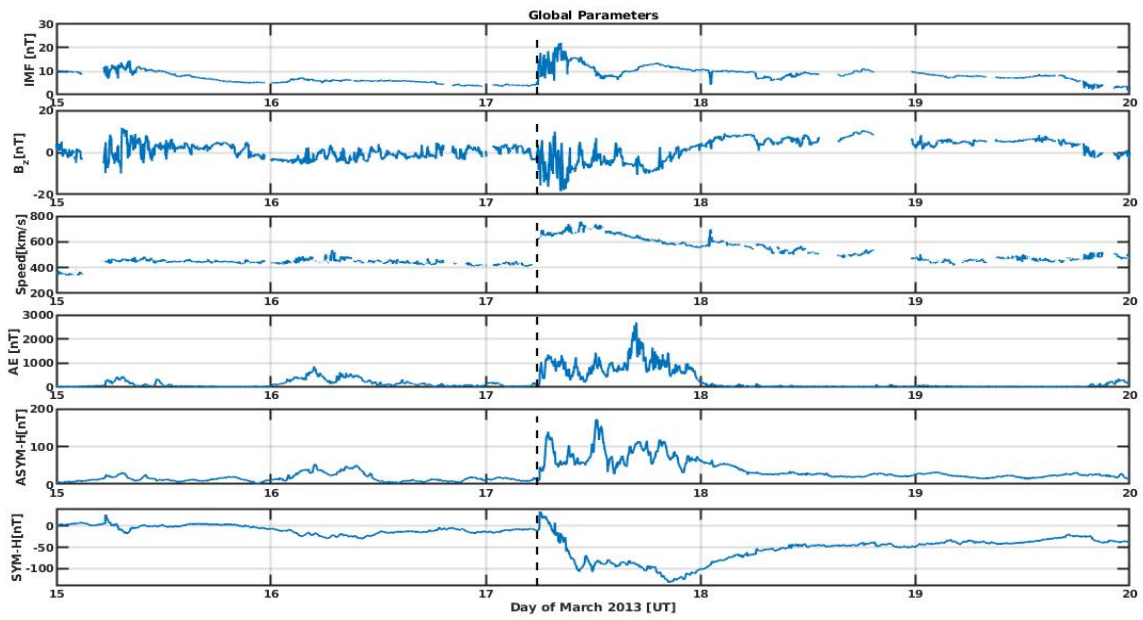
CME	Asia [07:00 LT] Africa [12 :30 LT] America [10 :30 LT]	91 02 Hours	08 Hours	(1491) 20041108-0830 (1753) 20041108-1030 (1629)		2.8 Days	4 Days	3.5 Days	-90nT	-74nT	<b>-70 nT</b>
Storm 13 Multiple CME	2004-07-22-0955 UT Asia [02:30 LT] Africa [08 :30 LT] America [06 :30 LT]	2207 1422 UT 27 08 Hours	2707 1335 UT -208 nT 05 Days	20040722-2130 (1284 nT) 20040723-0830 (1102) 20040723-1630 (1455)	4.5 Days	24/7 1300 27/7 0600 3.5Days 27/7 2000 29/7 2200 2.1Days	24/07 1300 26/07 1100 1.8Days 26/7 1800 28/7 2000 1.8 Days	24/7 1100 26/7 1300 2.1 Days 26/7 2100 28/7 1100 1.5 days	26/07/04 0215UT -100nT	27/07/04 1500UT <b>-127.4</b>	27/07/04 1600UT -60nT
Storm 14 CME	2001-09-23-0750 UT Asia [1430 LT] Africa [0630 LT] America [0330 LT]	2309 0935 UT 18 01 Hours	2309 1853UT -90 nT 10 Hours	20010923-1730 (1260)	01 Days	NA	NA	NA	23/09/01 0110UT -29nT	23/09/01 1730UT -37.9nT	23/09/01 1910 <b>-46nT</b>
Storm 15 CME	2003-11-20-0746 UT Asia [1430 LT] Africa [0630 LT] America [0330 LT]	NA	2011 1816UT -488 nT 10 Hours	20031120-0830 (1204) 20031120-1330 (1660) 20031120-1630 (1700)	04 Days	NA	20/11 1700 22/11 1900 2.1 Days	21/11 0200 21/11 2300 0.8 Days	NA	20/11/03 1930UT <b>-187nT</b>	20/11/03 2110UT -130nT
Storm 16	2000-10-03 2340UT Asia [0700 LT] Africa [2210 LT] America [2000		0510 1310 -180 nT 1.5 Days	20001004-0830 (888) 20001005-0630 (1260)	4.5 Days	NA	NA	NA	NA	NA	NA

	LT]										
Storm 17 CME	2001-11-24-0445 UT Asia [12 :00 LT] Africa [03 :30 LT] America [01 :15 LT]	24/11 0600 UT 74 02 Hours	24/11 1430 -230 nT 8.5 Hours	20011124-0630 (2006)	04 Days	24/11 1500 25/11 1700 1.1 Days	24/11 0500 25/11 1500 1.4 Days	24/11 0500 25/11 0700 1.2 Days	24/11/01 1210UT -60.64nT	24/11/01 1514UT <b>-111nT</b>	24/11/01 1624UT -77.79 nT
Storm 18 CME	2013-03-17-0406 UT Asia [12 :30 LT] Africa [04 :00 LT] America [02:30 LT]	17/3 0605 UT 32 02 Hours	2013,03,17,1723 UT -127 nT 11 Hours	20130317-1630 (1820)	03 days	NA	17/03 0500 18/03 1800 1.5 Days	17/03 0500 18/03 1500 1.4 Days	19/03/13 0340UT -13.4nT	17/03/13 1944UT <b>-87.3nT</b>	17/03/13 2010UT -83.4nT
Storm 19 HSSW	11 April 2005 0945 Asia [02:30 LT] Africa [08 :30 LT] America [06 :30 LT]	11/4 1634UT 25 07 Hours	2005,04,12,0540 -80 nT 09 hours	200504120330 (875) 200504121930 (855) 200504131230 (960) 200504131630 (1100)	06 days	12/4 2200 17/4 0000 3.1 Days	13/4 / 0100 15/4/ 0800 2.3 Days	12/4 1600 15/4 0300 2.5 Days	14/04/05 0245UT -22nT	14/04/05 0900UT <b>-48.58nT</b>	13/04/05 1730UT -24.5nT

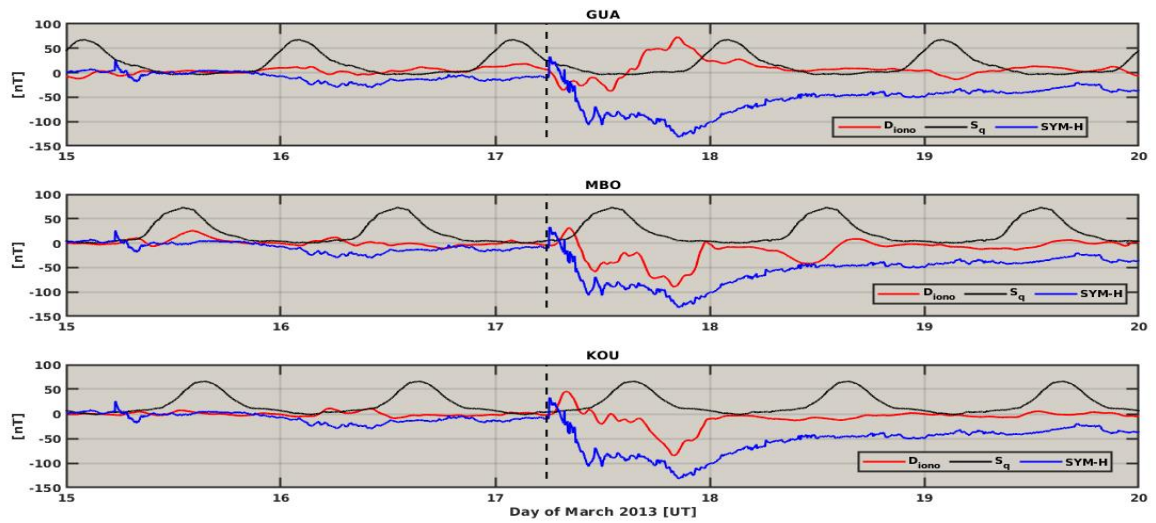




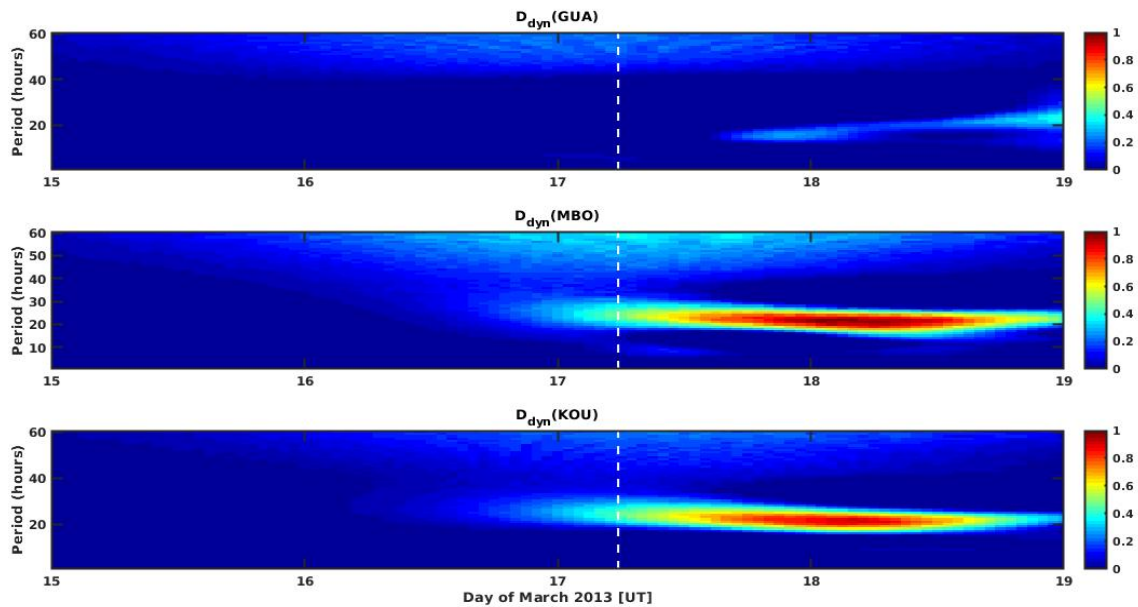
a)



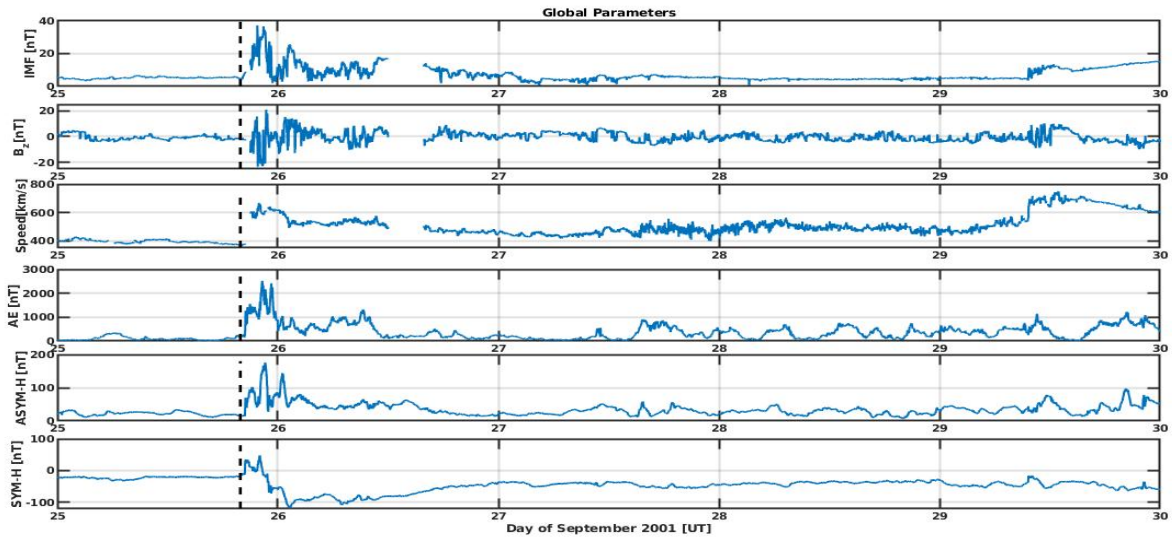
b)



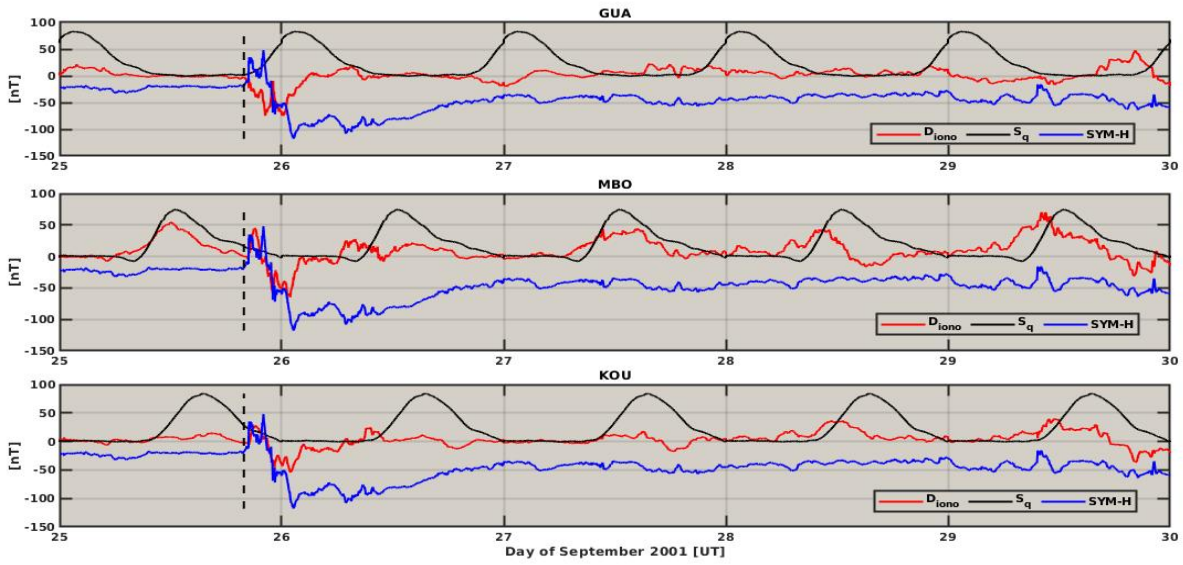
c)



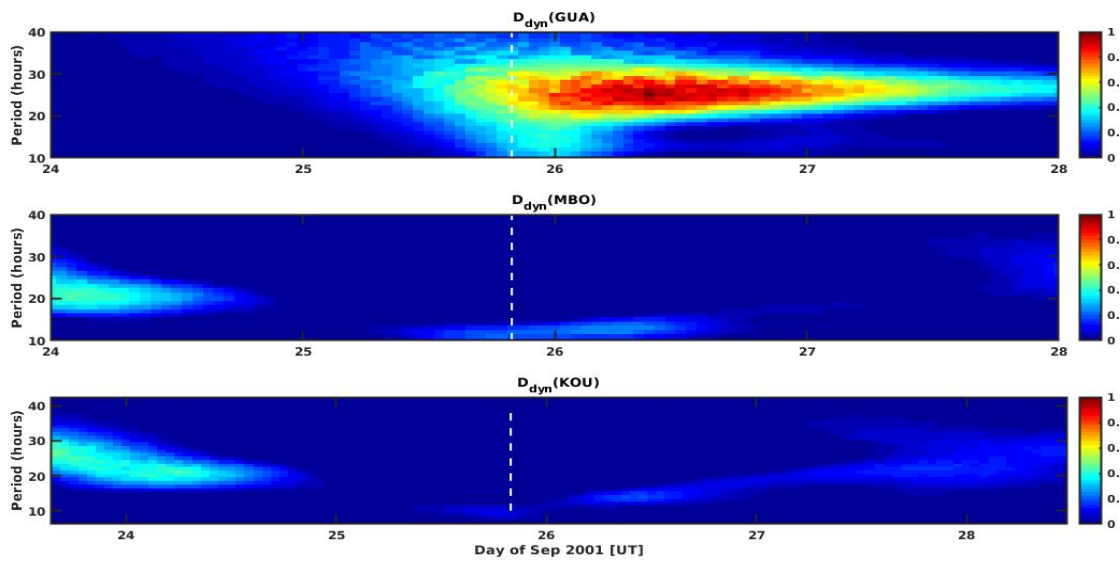
a)

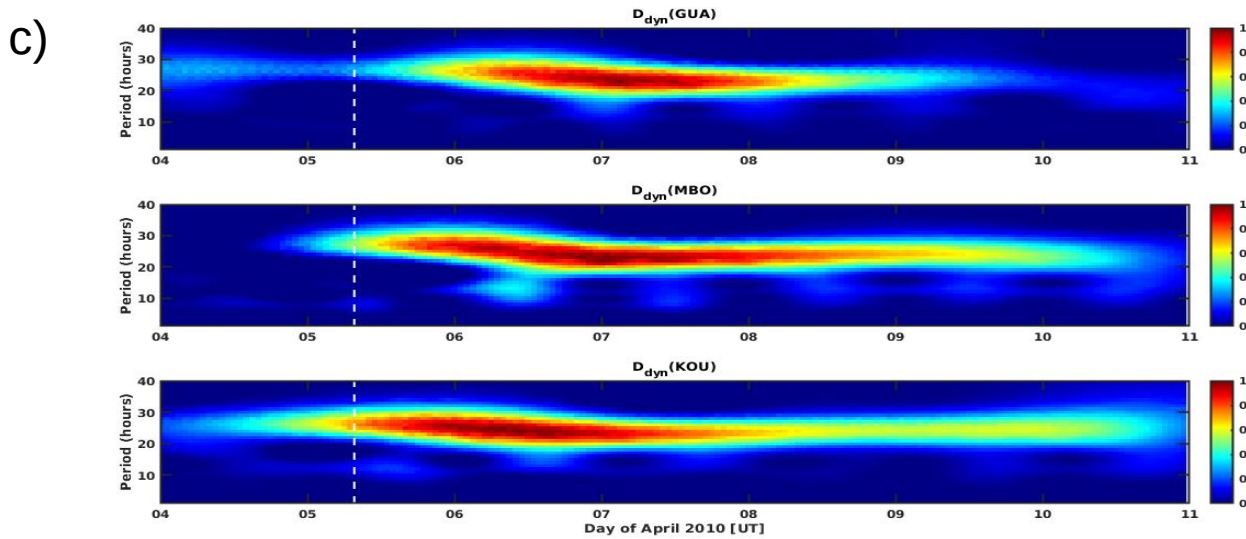
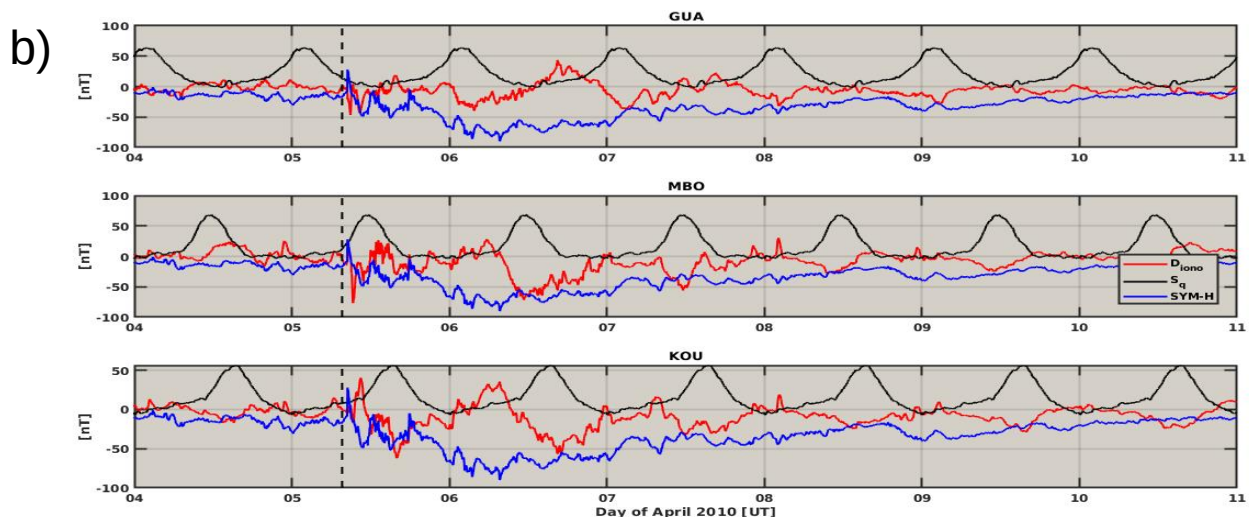
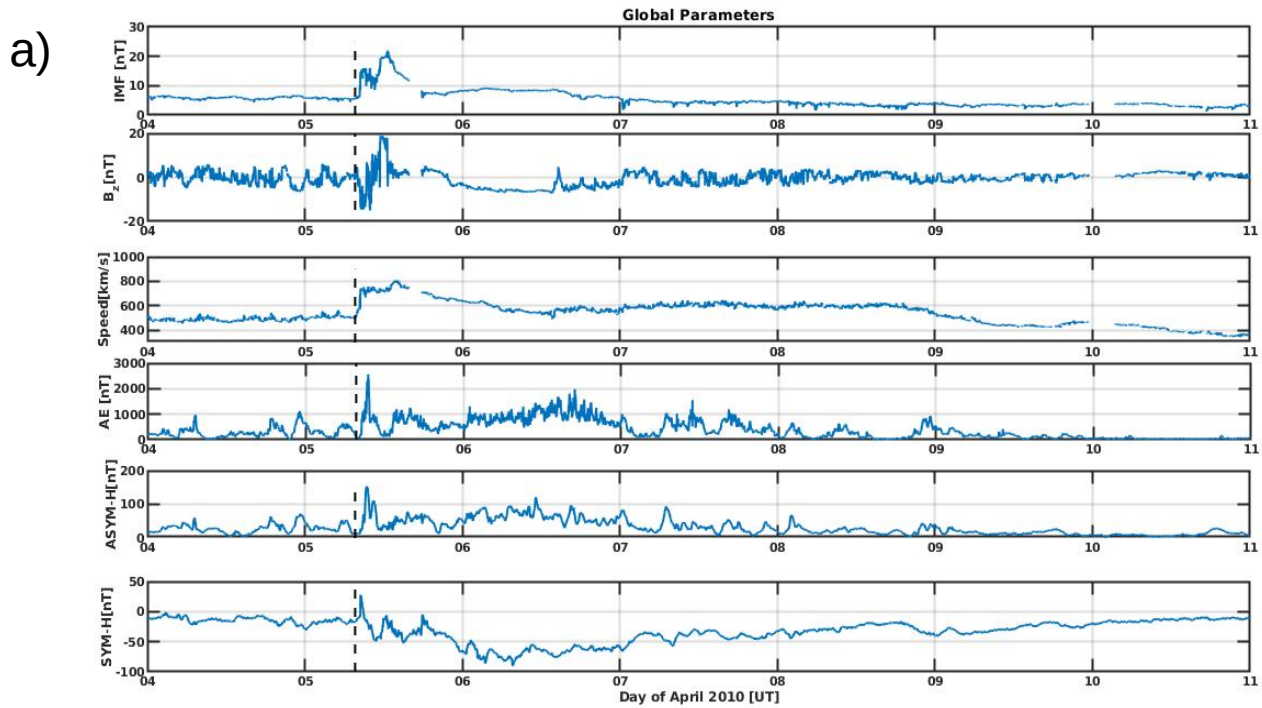


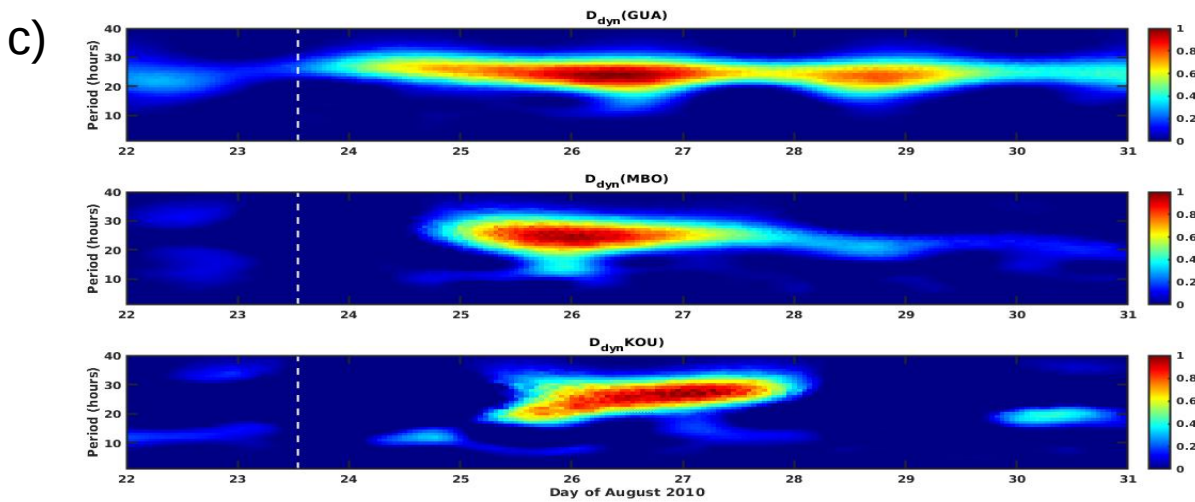
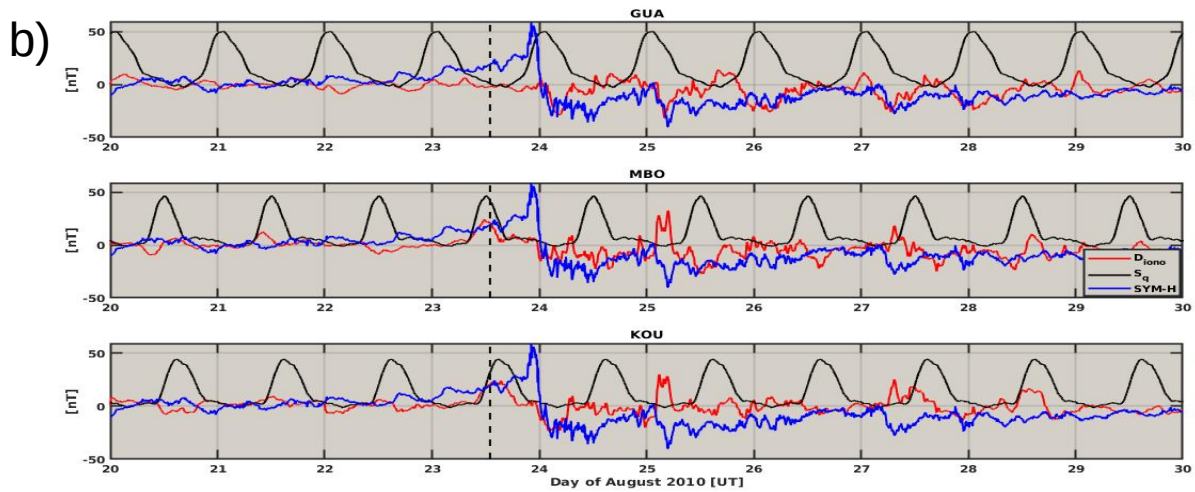
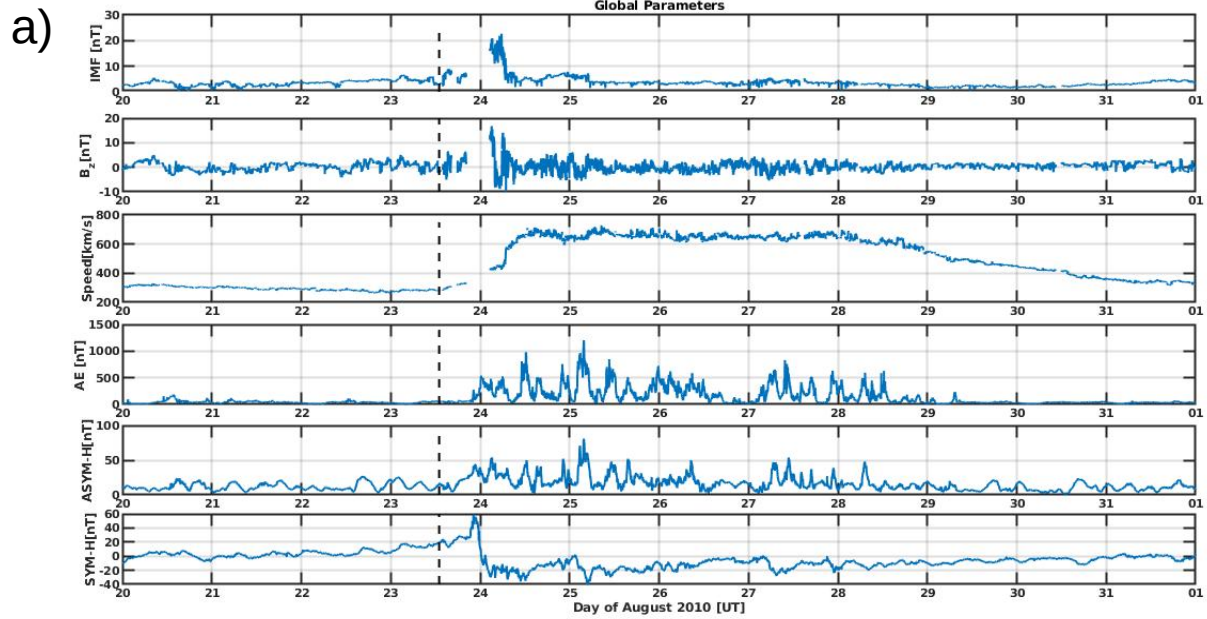
b)

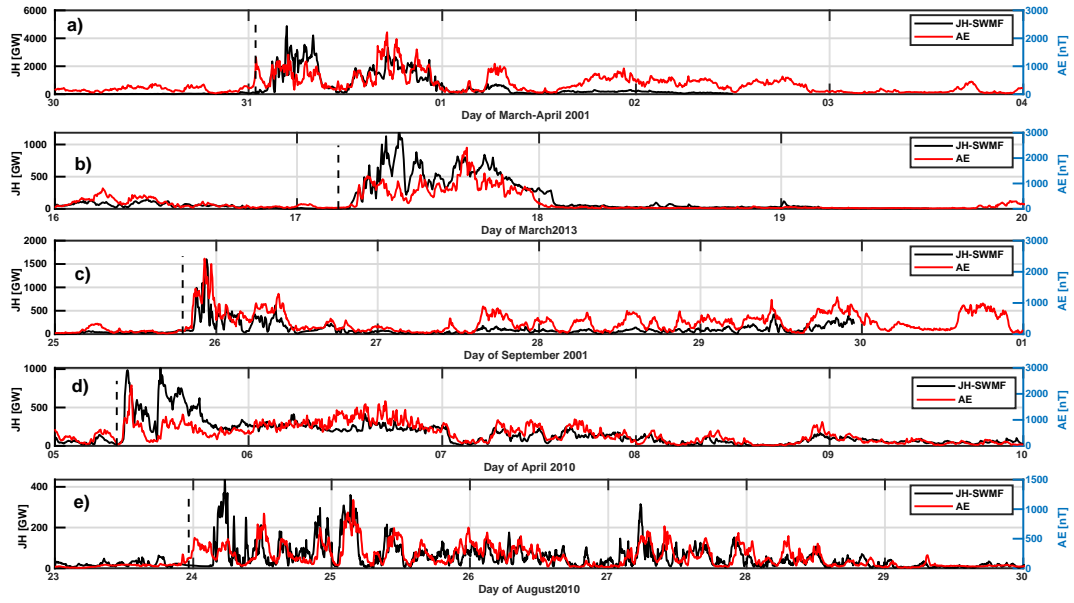


c)

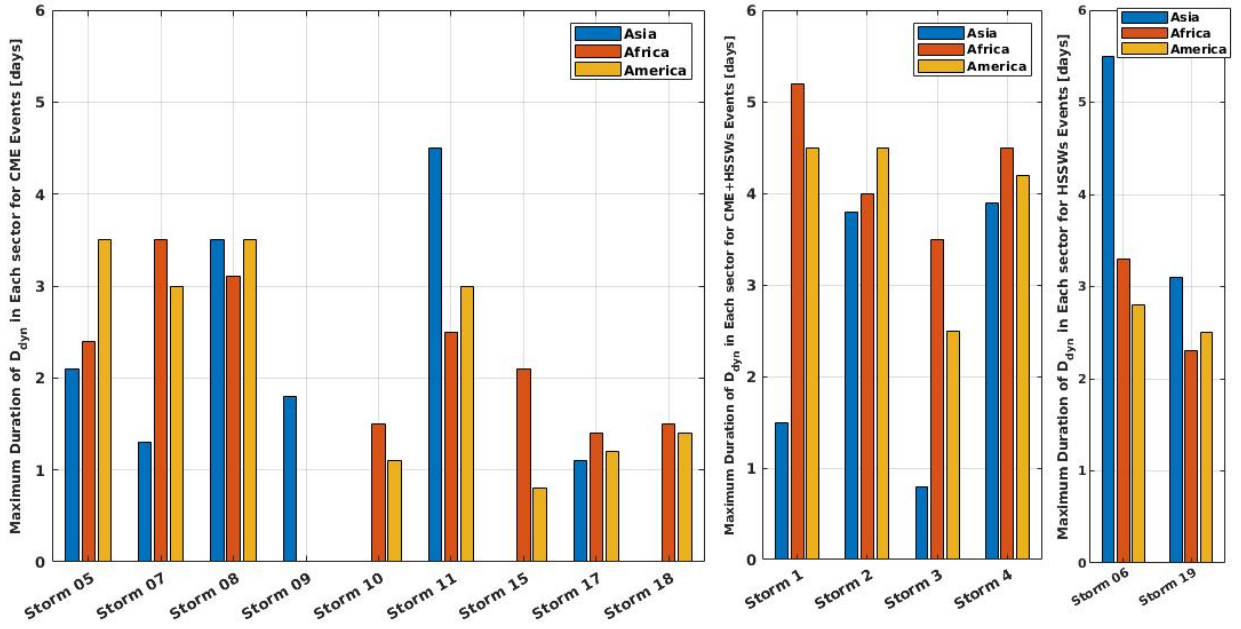




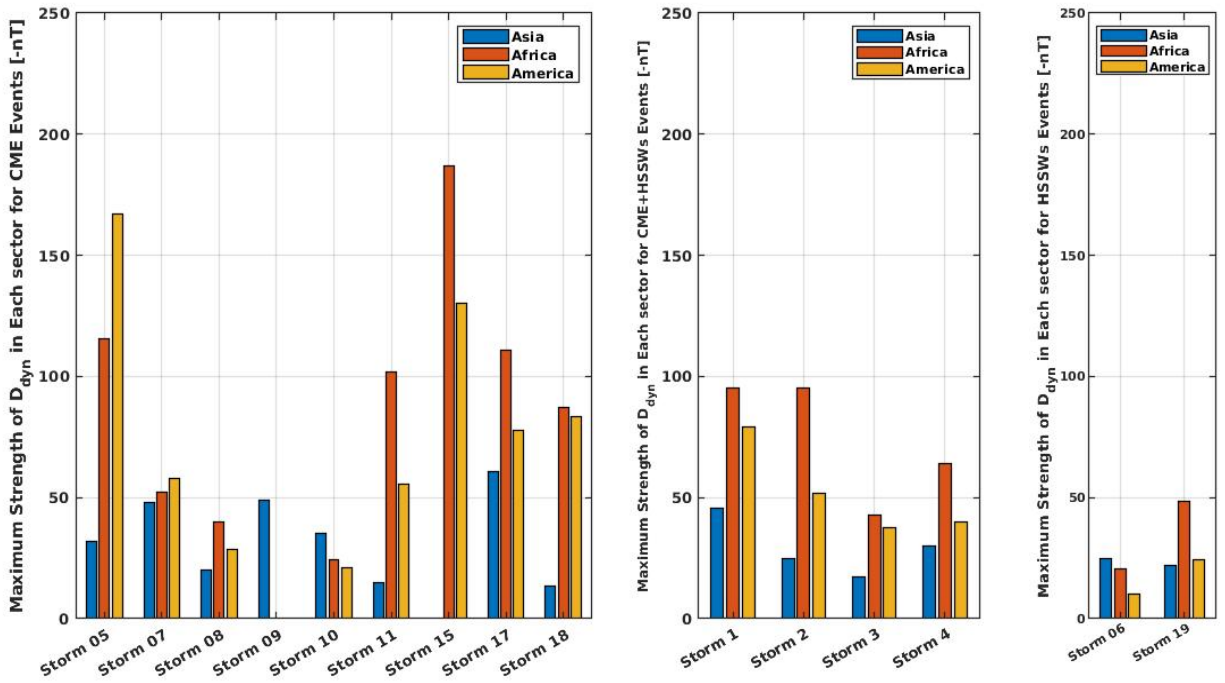




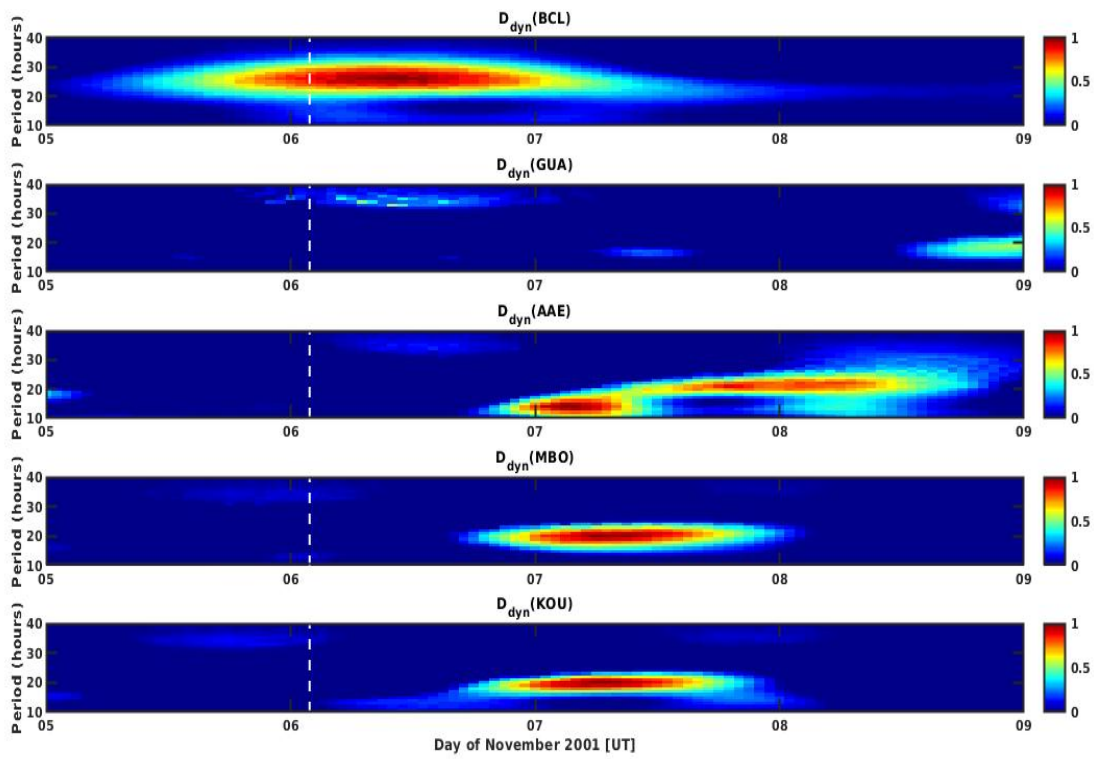
a)



b)



a)



b)

